# Another mode of decay of $M^*_{\mu\pi}(0.429)$

C. A. Ramm
*Department of Physics, University of Melbourne, Parkville, Victoria, Australia 3052*
(Received 27 June 1983; revised manuscript received 19 February 1985)

Experimental evidence for the narrow $(\mu,\pi)$ state $M^*_{\mu\pi}(0.429)$ is reviewed, including the observations of three groups of authors who have reported that there is no evidence. In seven independently calibrated $M_{\mu\pi}$ distributions an upward fluctuation located at 0.429 GeV within the errors of measurement is surrounded by lobelike patterns. The probability that the similarities of the patterns in the various experiments are caused by statistical fluctuations is negligible. No other known effects can account for them; the only quantitative explanation that has been found is that the lobes are due to another mode of decay of $M^*_{\mu\pi}$ involving a daughter particle $(M^{*\pm}_{\mu\nu})$. There is a rapid cascade, $M^*_{\mu\pi}\rightarrow(\mu_1,M^*_{\mu\nu})$, $M^*_{\mu\nu}\rightarrow(\mu_2,\nu)$; the neutral combinations $(\mu_1,\mu_2)$, incorrectly assigned as $(\mu,\pi)$, produce lobes symmetrically disposed around the $M^*_{\mu\pi}$ enhancement. The observations from $\nu$ experiments can be simulated to the limits of experimental error if $M^{\pm}_{\mu\nu}$ have a mass of $0.127\pm0.005$ GeV and a width of $0.005\pm0.003$ GeV and if in the c.m. system of $M^*_{\mu\nu}$ there is a preferential alignment of $\mu_2$ with $\mu_1$. The rate of decay of $M^*_{\mu\pi}$ via $M^*_{\mu\nu}$ is between 2.5 and 5 times that via $(\mu,\pi)$. It is to be expected that $M^*_{\mu\pi}$ produced in $K^0_{\mu3}$ has the same decay mode because of the strong correlation between the $M_{\mu\pi}$ distributions. Methods of analysis, a phenomenology of patterns in $M_{\mu\pi}$ distributions, searches for other causes of the patterns, and possible connections with other studies are described.

## I. INTRODUCTION

In $M_{\mu\pi}$ distributions from $\nu_\mu$ interactions, and from $K^0_{\mu3}$ decays, there is an enhancement from the production and decay of the short-lived particle

$$M^*_{\mu\pi}(0.429)\rightarrow(\mu^-,\pi^+)\ . \tag{1}$$

Some phenomenology of this decay has been given in a previous report,[1] further referenced as (I), where it is shown also that there is a correlation in the fluctuations near the $M^*_{\mu\pi}$ enhancement in $\nu$ and $K^0_{\mu3}$ bubble-chamber experiments. This report considers phenomenologies of $M_{\mu\pi}$ distributions in the vicinity of 0.429 GeV from eleven different experiments, including three from authors who have reported that they found no evidence for the existence of $M^*_{\mu\pi}$. It will be seen that the $M^*_{\mu\pi}$ enhancement is commonly surrounded by lobelike patterns which cannot be dismissed as statistical fluctuations or experimental errors. The only quantitative explanation which can be found for the collectivity of these observations is another mode of decay of $M^*_{\mu\pi}$, via a daughter particle whose decay products have not been separated from decay (1).

Phenomenological studies of the various distributions have extended over a considerable time: they will be summarized mostly in chronological order, so as to indicate the steps in their synthesis.

## II. $M_{\mu\pi}$ DISTRIBUTIONS IN BUBBLE CHAMBERS

In histograms of the small numbers of $M_{\mu\pi}$ values from early $\nu$ experiments in bubble chambers, the $M^*_{\mu\pi}$ enhancement is the only significant feature in the range $M_{\mu\pi}<m_K$. More numerous data from $K^0_{\mu3}$ decays, also in bubble chambers, show an enhancement at the same mass, which appears in an unexpected pattern with two lobes of comparable amplitude, unlikely[2] to be statistical fluctuations. Until other $M_{\mu\pi}$ distributions were available this lobelike pattern might have been considered a peculiarity of $K^0_{\mu3}$ experiments in bubble chambers: two examples are shown in Fig. 1.

Histogram (a) is from the X4 experiment[3] in freon ($CF_3Br$) in the 0.5-$m^3$ version of the heavy-liquid bubble chamber (HLBC): the $K^0_L$ beam traversed the chamber in a thin-walled vacuum pipe. $V^0$ from $K^0_{\mu3}$ and $K^0_{e3}$ are recognized efficiently in $CF_3Br$ because of the radiation length of $\sim11$ cm. The other $V^0$, without evidence of $\pi^0$ or $e$, are an almost pure sample of $(\mu,\pi)$ combinations from $K^0_{\mu3}$; (a) is from the well-measured tracks, less than half have any indication for identification as $\mu$ or $\pi$. So as to use the maximum information, (a) contains both unconstrained values of $M_{\mu\pi}$ from each $(\mu,\pi)$ regardless of scanning assignment. These dual entries, generally different, would tend to smooth any systematic experimental effects in the, expected, physically smooth $M_{\mu\pi}$ distribution. As in (I), a least-squares-fitted fourth-degree polynomial is shown in (a) as a reference[4] for smoothness. The heavier line indicates a lobelike pattern containing the $M^*_{\mu\pi}$ enhancement. It was noticed also that this pattern has the worst fit[2] to the reference of any corresponding range of $M_{\mu\pi}$. For the 18 bins indicated, $\chi^2_{18}=39.9$, corresponding to a confidence level (CL) of $10^{-3}$ for the hypothesis that the indicated region is physically smooth and represented by the reference. The confidence level for such an hypothesis will be shown as CLS, the $N$ in $\chi^2_N$ is the number of bins over which $\chi^2$ is calculated, the number of degrees of freedom is taken as $N-1$.

The contributions to this $\chi^2_{18}$ from the left-hand pair of bins, the bin at $M^*_{\mu\pi}$, and its left neighbor, and the right-

 

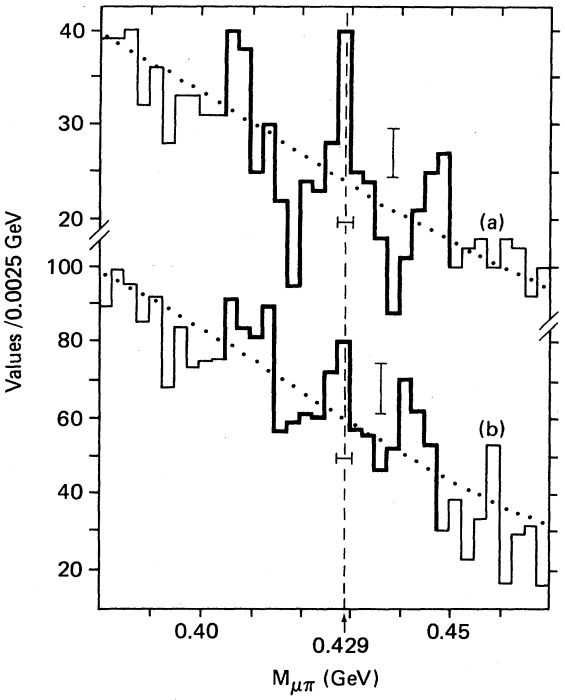


FIG. 1. Comparison of $M_{\mu\pi}$ distributions in the vicinity of 0.429 GeV from $K_L^0$ decays in (a) the HLBC and (b) the HBC. The scales of the ordinates are chosen so that physical structure from the $K_{\mu 3}^0 \rightarrow (\mu,\pi,\nu)$ decays would appear the same in each histogram. The horizontal bars here and in subsequent diagrams show the possible mean absolute error in $M_{\mu\pi}$ at 0.429 GeV. Essentially, this paper investigates whether the resemblances in the patterns around the $M_{\mu\pi}^*$ enhancement in these and other $M_{\mu\pi}$ distributions are due to statistical fluctuations, systematic errors, or physical causes.

hand pair of bins are $\chi^2{}_2=4.8$, 11.7, and 6.5 (CLS=3%, $10^{-3}$, and 1%), respectively. Without the seven bins centered on the $M_{\mu\pi}^*$ bin, $\chi^2{}_{11}=26.2$ (CLS$=3\times10^{-3}$). Thus the statistical significance of the lobelike features is comparable with those of the $M_{\mu\pi}^*$ enhancement. In order to assess whether the pattern is likely to be due to statistical fluctuations, or other errors peculiar to these observations, information was kindly made available from another experiment with a $K_L^0$ momentum spectrum similar to that in the HLBC. Histogram (b) is from a study[5] in the Brookhaven 14-in. hydrogen bubble chamber (HBC). The components of the $V^0$ are unidentifiable, the $M_{\mu\pi}$ are from both assignments, as for (a). In order to diminish background from $K_{e3}^0$ decays, $V^0$ with a resultant transverse momentum $(p_T)>0.1$ GeV/$c$ are rejected; this makes the remaining $K_{e3}^0$ contribution convex in the region of the diagram, and the true $M_{\mu\pi}$ distribution increasingly convex below 0.385 GeV, as will be seen in Fig. 2(d). The maximum value of $p_T$ at $M_{\mu\pi}^*$ is 0.064 GeV/$c$ from

$$T_\nu=(m_K{}^2-M_{\mu\pi}{}^2)/2m_K \ .$$

For convenience of comparison, the dotted reference of Fig. 1(b) has been given a slope similar to that in (a) by

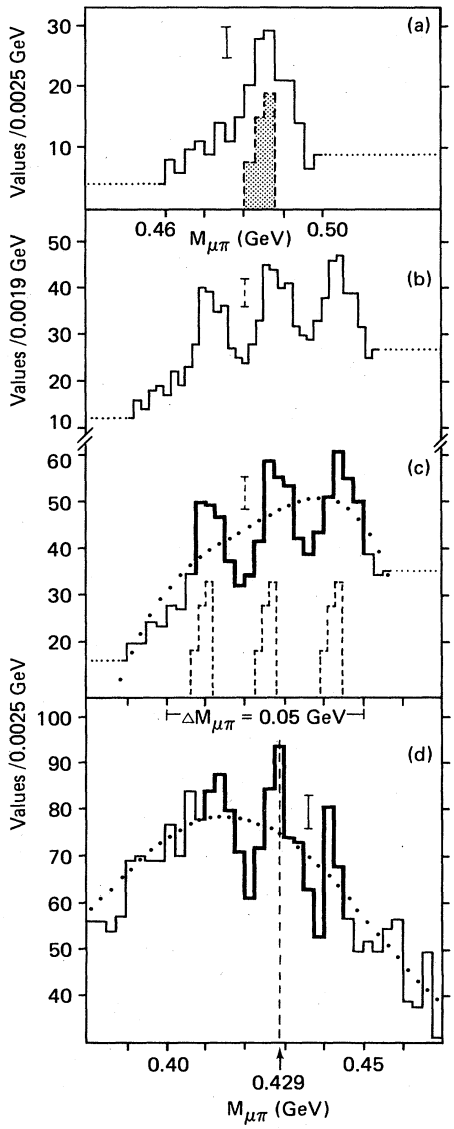


FIG. 2. Demonstration that an $M_{\mu\pi}$ distribution from three symmetrically spaced phenomena can have a pattern in the HBC similar to the indicated regions in Fig. 1. (a) Observed distribution of $0.46<M_{\mu\pi}<0.50$ GeV from all $V^0$ with $0.1<p_T<0.2$ GeV/$c$, assigned as $(\mu,\pi)$ and selected for $p_\mu=p_1$, $p_1/p_2<5$. The calculated feature from $V^0$ from $K_S^0\rightarrow(\pi,\pi)$, incorrectly assigned as $(\mu,\pi)$, is shaded (arbitrary vertical scale). For the making of a test pattern, histogram (a) is extended as shown, added to itself twice, each time displaced by nine bins. The result is shown in (b), scaled in $M_{\mu\pi}$ by the ratio of the $Q$ values for $M_{\mu\pi}=0.429$ and 0.487 GeV. Thus (b) could actually be an observed distribution in the HBC if there were three symmetrically spaced features near 0.429 GeV, each a scaled replica of the shaded feature caused by $K_S^0$ in (a). Histogram (b) has been converted to bins of 0.0025 GeV, assuming a uniform density of values across each bin, to produce the test histogram (c). This may be compared with (d), which is an actual $M_{\mu\pi}$ distribution from the HBC with $(\mu,\pi)$ selected as for (a), except here $p_T<0.1$ GeV/$c$, to accept $K_L^0$ decays and eliminate background significantly out of the beam direction. This test shows that the indicated region of (d) could be caused by three physical features spaced like the dashed features in (c).

subtraction from the data of a smooth $K^0_{e3}$ background, using an estimate of $2.49\pm0.26$ for the ratio of the $K^0_L$ decays in the HBC compared with the HLBC, and assuming the difference in the shapes of their polynomial curves is due to the $K^0_{e3}$ background. For (b) the polynomial is calculated for the range $0.355 < M_{\mu\pi} < 0.500$ GeV; i.e., above the region of the background from $K^0_{\pi 3}$. The ordinates are also proportioned with the factor of 2.49 thus, because of the similar acceptances in each experiment of the $V^0$ configurations, any physical structure in the $M_{\mu\pi}$ distribution from $K^0_{\mu 3}$ decays would appear of similar size in (a) and (b).

There are enhancements at $M^*_{\mu\pi}$ in each distribution and resemblances in the neighboring patterns. However, before the background subtraction, the indicated region of (b) is a statistically smooth fit to its polynomial: $\chi^2_{17}=12.1$ (CLS=73%). If the indicated region of (a) were scaled in amplitude to have the same reference level as that in the $M^*_{\mu\pi}$ bin in (b), a $\chi^2_{17}$ of 102 would be obtained for (b). From the data shown in (b), a numerical value of $\chi^2_{17}=34.5$ (CLS$=4\times10^{-3}$) is calculated. It will become apparent that a difference in size of the patterns can be caused by technical differences in the experiments, such as residual $K^0_{e3}$ background, absence of a beam pipe, and scanning criteria.

The coefficient of correlation[2] of the indicated region of (b) with histogram (a) gives a CL of 30% that both represent the same physical distribution. However, if the correlation is recalculated as the indicated region of (b) is displaced relatively to (a) in steps of one bin, after three steps in either direction the CL is $<10^{-3}$ [cf. also Fig. 8 of paper (I)]. Such a sensitivity to small displacements would not be expected for physically smooth distributions. However, neither indicated region has the appearance of an $M^*_{\mu\pi}$ enhancement on a physically smooth background, as would be expected if the $M_{\mu\pi}$ distributions were contaminated with a single decay.

It can be asked whether the stability of calibration of the absolute mass scale throughout these experiments, and the mass resolution in the measurement and the data reduction can allow any physical phenomenon to cause such patterns. In the HBC the $K^0_L$ traversing the beam window and other material produce $K^0_S$; their decays can be used for a direct test of the experimental resolving power. Figure 2(a) shows the $M_{\mu\pi}$ distribution[2] from all $V^0$ with $0.1 < p_T < 0.2$ GeV/$c$, assigned as $(\mu,\pi)$, with $p_\mu = p_1$ and selected for $p_1/p_2 < 5$. It has been shown previously that if the momenta of the tracks in a $V^0$ are labeled $p_1, p_2$ such that $p_1 > p_2$, the significance of the $M^*_{\mu\pi}$ enhancement is greater for the assignment $p_\mu = p_1$. This procedure also causes $K^0_S$ decays, incorrectly assigned as $(\mu,\pi)$, to contribute a narrow feature: the calculated appearance for perfect measurement is shown hatched. There is no other similar pattern from $K^0_S$, $\Lambda^0$ would contribute a feature at $M_{\mu\pi}\sim0.45$ GeV, and the end point of $K^0_{\pi 3}$ appears at $M_{\mu\pi}\sim0.35$ GeV; for $p_T<0.1$ GeV/$c$ the contributions for $K^0_S$ and $\Lambda^0$ are negligible. The calculated feature in (a) is directly under the peak in the $M_{\mu\pi}$ distribution, as is to be expected from the calibration by direct observation of $K^0_S$ and $\Lambda^0$ during the same experiment. This situation can be compared with a similar observation by Clark *et al.*[6] of the $M_{\mu\pi}$ distribution from $K^0_S$ assigned as $(\mu,\pi)$ in an experiment which detects the symmetrical $(\pi,\pi)$ configuration. The corresponding peak in their distribution is within the range of the dotted feature in Fig. 2(a), near to the low mass limit, as is to be expected; the large values of $p_\mu/p_\pi$ contribute the upper mass limit of the feature.

As described in the caption for Fig. 2, the observed distribution in (a) can be used to produce an experimentally significant test pattern which shows that the stability of mass calibration throughout the HBC experiment does permit a physical distribution of three similarly spaced features, of natural spread at least as great as 0.005 GeV as shown in (c), to cause an indicated region such as in Fig. 1. A sharp decay, as distinct from the broad feature from incorrectly assigned $K_{\pi\pi}$ would, of course, produce a pattern of still greater amplitude than that in Fig. 2(c). For the indicated region of Fig. 2(c), $\chi^2_{17}=26.8$ (CLS=4%) and for (d), $\chi^2_{14}=19.8$ (CLS=10%). A similar direct test is not possible for the HLBC because the purpose of the beam pipe was to preclude such $K^0_S$ production. It is known from the X4 studies that the error in the mean absolute mass scale is $<0.002$ GeV, and that the mass resolution is comparable with the HBC.

In an experimental determination of invariant masses the resolution function for a sharp decay may be considered as the sum of the resolution functions for mass measurements from various types of configurations of the decay. Even if individually these contributing functions were normal distributions, their sum would not be in general a normal distribution. Some experimental situations, such as a dependence of the mean measured mass on whether the tracks of a $V^0$ are opening or crossing, can cause bimodal mass distributions. Multimodal distributions can be caused by shifts in mass scale calibration. Thus in considering possible causes of fluctuations near $M^*_{\mu\pi}$ it is desirable to have as reference a distribution of observed mass measurements of a known phenomenon, rather than a predicted resolution function, in order to verify that with the bin widths of the $M_{\mu\pi}$ histograms the observed distribution from decay (1) cannot be, itself, multimodal. When the measured invariant mass from a sharp decay is sufficiently independent of the position of the decay in the apparatus, configuration, methods of measurement (e.g., curvature of tracks or range) and time, and the smaller variances predominate in the distribution of the estimated variances of the mass measurements, the observed mass distribution is more sharply peaked than a normal distribution calculated from the average of the range of mass errors. This situation obtains in the HLBC, HBC, and other experiments to be considered shortly. The preferred orientation of the $M^*_{\mu\pi}$ decay to the line of flight (LOF), the lower $Q$ value, and the smaller average nuclear scattering in tracks of $(\mu,\pi)$, contribute to sharper peaking of the observed $M^*_{\mu\pi}$ mass resolution function than that from the isotropic decay: $K^0_S\rightarrow(\pi,\pi)$.

## III. COMPARISON WITH SPARK-CHAMBER OBSERVATIONS

The similarities of shape and location of the patterns in Fig. 1 seemed unlikely to be defects from the measure-

ment of invariant masses, or a coincidence of statistical fluctuations: for a long time no other explanation could be offered. More prolific data from a spark-chamber (SC) experiment were kindly made available.[7] For the restricted $K^0_{\mu 3}$ decay configurations detectable in electronic experiments, the short-term mass resolution can be superior to that in bubble chambers; long-term stability of the mass scale is more difficult to achieve. It was soon found that the $M^*_{\mu\pi}$ enhancement and indications of neighboring patterns were visible in some runs of the SC, but are not recognizable in the $M_{\mu\pi}$ distributions from the total data, regardless of kinematical selections which had been developed for the HBC; also the small $K_{\pi\pi}$ signal was asymmetrically distributed about $m_K$. Figure 3(a), which is a $M_{\mu\pi}$ distribution from the $V^0$ of all runs, assigned as $p_\mu = p_1$, typifies this situation. There are no recognizable patterns in the statistically smooth distribution; for 19 bins centered on the $M^*_{\mu\pi}$ bin: $\chi^2_{19} = 16.5$ (CLS = 56%). The range for calculation of the polynomial is the same as for the HBC.

The fact that the $M^*_{\mu\pi}$ enhancement was identifiable in any runs led to an extensive investigation. It became clear that sporadic changes in calibration of the mass scale which are too small to affect the primary aim of the experiment, to study form factors, prevent the formation of any pattern containing the $M^*_{\mu\pi}$ enhancement. There are insufficient $K_{\pi\pi}$ in the SC for calibration of the mass in individual runs; it was found that an average momentum correction can be assigned to individual runs, according to the observed upper limit of the $M_{\pi\pi}$ distribution from $K^0_{\pi 3}$. Completely efficient retrospective correction is impossible, however, those sequences of consecutive runs which have similar average corrections give the distribution in (b). The upward fluctuation in the $M^*_{\mu\pi}$ bin is 4.2 standard deviations (SD); i.e., for this distribution a statistical fluctuation of such a magnitude has a probability $< 10^{-4}$ of appearing in any bin, and $< 10^{-5}$ of simulating the $M^*_{\mu\pi}$ enhancement. The probability is negligible ($< 10^{-10}$) that a fortuitous selection of corrections would produce such a result from subsets of the data of (a) and, simultaneously, make their $K_{\pi\pi}$ signal symmetrical about $m_K$. The pattern around the $M^*_{\mu\pi}$ enhancement is not recognizable, immediately, as that in the same region in Fig. 1; some similarities will be indicated shortly. This study[8] gave further confirmation of the existence of the $M^*_{\mu\pi}$ enhancement with a mass compatible with $0.429 \pm 0.002$ GeV, previously determined from the HLBC and HBC. A demonstration of smoothing from shifts in mass scale calibration is also in Fig. 3. In an actual experiment the fluctuations in calibration would render the demonstrated pattern more diffuse than in Fig. 3(d) because of the excursions of the instantaneous corrections from the run averages.

With experiments which accept only small ranges in $M_{\mu\pi}$ and which have, therefore, references which are more curved than in Fig. 1, any patterns they may have are better compared in histograms of the differences between the observations and the reference, rather than in a sloping histogram. So that the particular choice of degree of the polynomial is objectively unimportant the differences shown will be the averages from four polynomials

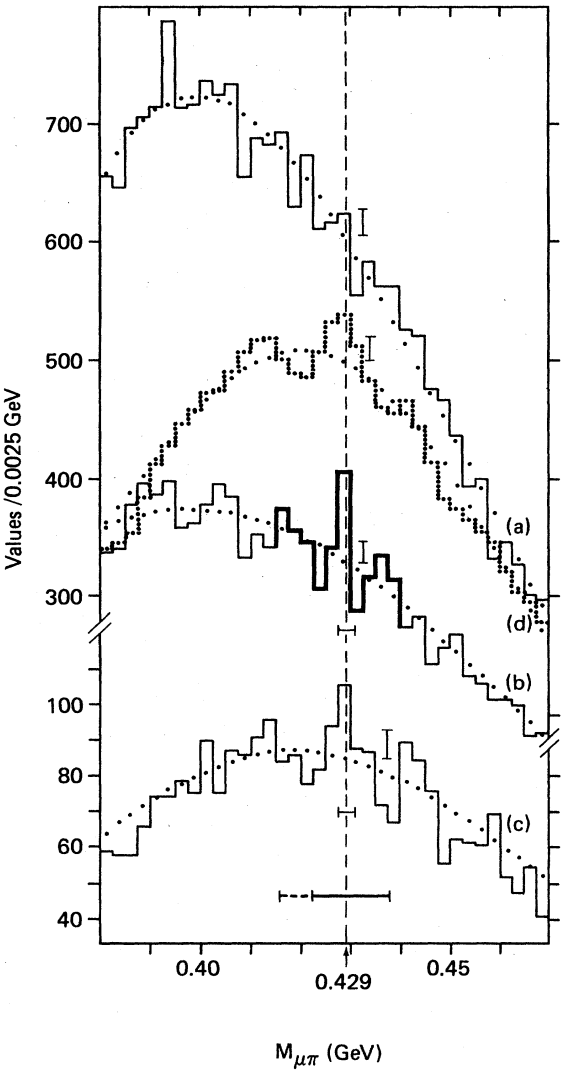


FIG. 3. Effects of fluctuations in calibration. Histograms (a) and (b) demonstrate the detection of the $M^*_{\mu\pi}$ enhancement by calibration of the mass scale. (a) The statistically smooth $M_{\mu\pi}$ distribution for the $p_\mu = p_1$ assignment of the $V^0$ from all runs of the SC; (b) $M_{\mu\pi}$ distribution from those sets of three or more consecutive runs in (a) with similar mass scale corrections as determined from $K^0_{\pi 3}$. For the indicated region: $\chi^2_{10} = 29.4$ (CLS $= 6 \times 10^{-4}$); the fluctuation in the $M^*_{\mu\pi}$ bin is 4.2 SD with respect to the dotted polynomial. For this enhancement and two bins either side: $\chi^2_5 = 25.2$ (CLS $= 5 \times 10^{-5}$). The probability is negligible that a random choice of correction factors would transform subsets of the data of (a) into (b). Histograms (c) and (d) demonstrate the smoothing of the $M^*_{\mu\pi}$ pattern by mass-scale fluctuations. (c) $M_{\mu\pi}$ distribution from $p_\mu = p_1$ from HBC; (d) addition of distributions of (c) each displaced by the individual corrections used for (b). Instead of the $M^*_{\mu\pi}$ enhancement being $\sim 5$ SD, it is less significant than in (c), and the lobes are almost unrecognizable. The lowest solid horizontal bar shows the range of the corrections for (b), the dashed extension includes all corrections determined from (a).

(two odd and two even), of consecutive degrees higher than where the reduction in $F$ value is statistically significant. A bar at zero on the ordinate shows the spread of the four polynomials which are, of course smooth, but not coincident or parallel. Thus histogram (a) in Fig. 4 shows the averaged differences between the observations in Fig. 3(a) and the level at the center of each bin of the weighted, least-squares fitted polynomials of degree 4, 5, 6, and 7. The error bar is 1 SD for the average reference level in the $M^*_{\mu\pi}$ bin. Similarly, histogram (b) is from Fig. 3(b): the discrepancies between the information of Fig. 3, where the polynomials are fourth degree and unweighted, are unimportant; e.g., for the indicated region of Fig. 4(b), $\chi^2{}_{10}=29.1$, to be compared with $\chi^2{}_{10}=29.4$ for Fig. 3(b). For averaging with respect to polynomials of degrees 10, 11, 12, and 13, $\chi^2{}_{10}=27.9$; the lower value is due to the increased accommodation with respect to the significant $M^*_{\mu\pi}$ enhancement.

Bisi *et al.*[9] reported that in an experiment to study two-body decays of $K^0_L$, and decays of coherently regenerated $K^0_S$, they found no evidence of $M^*_{\mu\pi}$. In the region of $M^*_{\mu\pi}$ their distributions have a level some tenfold the combined data of the HLBC, HBC, and SC; therefore if $M^*_{\mu\pi}$ were produced isotropically in the $K^0_{\mu 3}$ center-of-mass system (c.m.s.) and decayed isotropically with respect to its own line of flight, a large signal could be expected. The apparatus of Bisi *et al.* is designed to detect the symmetrical decay configuration of $V^0$ from two-body decay of $K^0_L$; i.e., for $K_{\pi\pi}$, equal and opposite transverse momenta of 0.206 GeV/$c$ for which, of course, $p_T=0$. The $M_{\mu\pi}$ are from a zero-constraint fit to $K^0_{\mu 3}$ with two possible solutions; when acceptable both are included in data I. This procedure differs from the dual entries in Fig. 1 and the $p_\mu=p_1$ of Figs. 2 and 3. With procedures involving the quadratic ambiguity, such as for data I, it is not obvious where the alternative solutions for $M_{\mu\pi}$ are situated.

Difference histogram (c) in Fig. 4 is from that part of data I for which[9] $\cos\theta_{\mu\nu}<0$; $\theta_{\mu\nu}$ is the angle between the $\mu$ and $\nu$ momenta in the $K^0_{\mu 3}$ c.m.s., where Bisi *et al.* conjectured that some effect of alignment might be observable: that part of data I for which $\cos\theta_{\mu\nu}>0$ shows a less significant pattern near $M^*_{\mu\pi}$. For convenience of comparison here, the bins of 0.0025-GeV in $T_\nu$ of the original data, shown in the Appendix, section 2, have been converted to bins of 0.0025 GeV in $M_{\mu\pi}$. The smaller vertical error bar shows the rms reading error, determined from successive measurements of the original diagrams, the horizontal error bar is the calibration error, the differences are averaged with respect to polynomials of degree 10, 11, 12, and 13, appropriate to the data range of $0.370<M_{\mu\pi}<0.500$ GeV. For the indicated region, $\chi^2{}_{21}=40.9$ (CLS$=4\times10^{-3}$). The level of the reference in the $M^*_{\mu\pi}$ bin in this sample of data I is 7.4 times the corresponding level of Fig. 4(a), ($\chi^2{}_{19}=16.5$); and 1.7 times the level of the data, to be discussed shortly, for (d) where $\chi^2{}_{21}=13.1$ It might be expected that if the $M_{\mu\pi}$ distribution in the indicated region of (c) were physically smooth, the test of the degree of smoothness (CLS$=4\times10^{-3}$) would be no less confirmatory than the indications from the less prolific data for (a) (CLS$=56\%$) and (d)

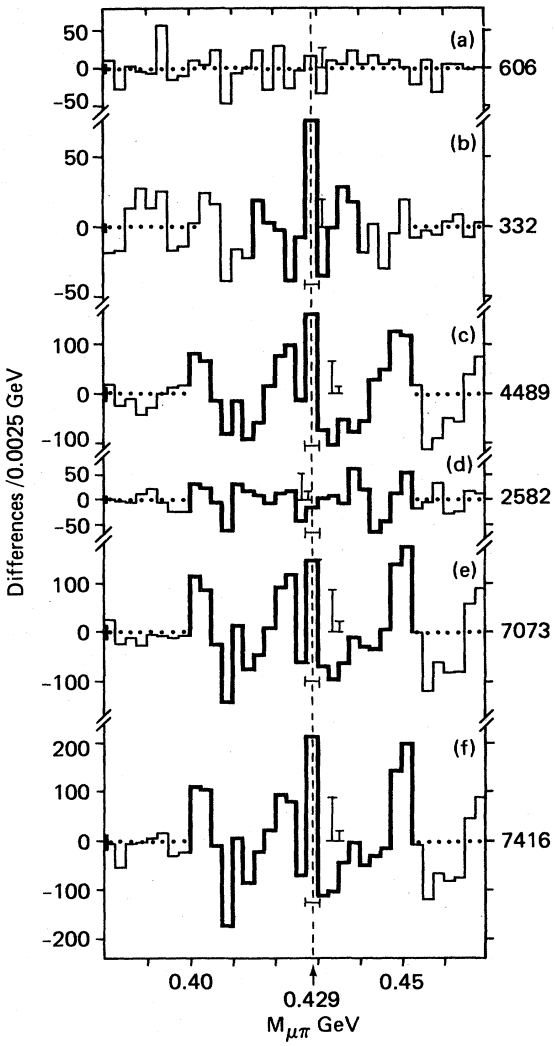


FIG. 4. The region of $M^*_{\mu\pi}$ in three-spark-chamber $K^0_{\mu 3}$ experiments. (a) shows the difference between the observed $M_{\mu\pi}$ histogram in Fig. 3(a) and the polynomial reference in each bin, averaged for references of four successive degrees (see text), the figure to the right of the zero line is the average level of the references in the $M^*_{\mu\pi}$ bin; (b) is obtained correspondingly from Fig. 3(b); the indicated region in that diagram is recognizable here. Data I from Bisi *et al.* are used to obtain (c), the errors in the mass scale are $<0.003$ GeV. There is an upward fluctuation in the $M^*_{\mu\pi}$ bin and a resemblance with the patterns in Fig. 1: $\chi^2{}_{21}=40.9$ (CLS$=4\times10^{-3}$). The data of (c) cannot be considered to demonstrate smoothness in the region of $M^*_{\mu\pi}$, particularly as they are more numerous than the statistically smooth data for (a) for which $\chi^2{}_{19}=16.5$ (CLS$=56\%$), and (d) from Clark *et al.* for which $\chi^2{}_{21}=13.1$ (CLS$=91\%$). There is no $M^*_{\mu\pi}$ fluctuation in (d) because only $(\mu,\pi)$ with $p_T\sim0$ are accepted. The addition of the data for (c) and (d) is used for (e); and the addition of the data for (b), (c), and (d) for (f) where $\chi^2{}_{21}=41.5$ (CLS$=3\times10^{-3}$), i.e., this indicated region can be considered less smooth than the same region of any one of (b), (c) or (d). The $M^*_{\mu\pi}$ enhancement and the symmetrically located lobes in (f), from the combined observations of the three spark-chamber experiments, have an obvious resemblance with the patterns in the histograms in Fig. 1 and the difference histograms shown in Figs. 6(a) and 6(b).

(CLS=91%). Bisi *et al.* do not explain why this prolific data set is not smooth. This observation, in a study to investigate a claim that $M_{\mu\pi}$ distributions in the region of 0.429 GeV are not smooth, does not substantiate their conclusion that there is no evidence for such a claim.

Bisi *et al.* state a mass resolution of 0.003 GeV near 0.429 GeV for data I: a report on a search[10] for $K_L^0 \to (\mu,\mu)$ with the same apparatus shows a histogram of $\sim 10^4 M_{\pi\pi}$ with a full width at half height of 0.010 GeV and a clear peak in the bin $0.496 < M_{\pi\pi} < 0.498$ GeV. This demonstrates that the absolute mass scale calibration is satisfactory and that the overall mass resolution function is unimodal and sharply peaked. Evidently, the $M_{\pi\pi}$ distribution appropriate to data I can be used also as the basis of the test in Fig. 2, instead of the $M_{\mu\pi}$ assignment of the $(\pi,\pi)$, which was chosen there as an example of an experimental observation of a feature with significant and calculable width. From such a test it would be concluded that data I would show a narrow upward fluctuation at $M^*_{\mu\pi}$ and similarly narrow lobes. The extent to which this distribution would be observed in an experiment would depend on the acceptance of the configurations of the $V^0$ from $M^*_{\mu\pi}$ and, the similarity of the operating conditions in the $K_L^0 \to (\mu,\mu)$ and the $K^0_{\mu 3}$ experiments.

There is an upward fluctuation in the $M^*_{\mu\pi}$ bin in (c), as would be expected from the test, and the pattern in the indicated region has resemblances with the patterns in Fig. 1. An obvious difference is the asymmetry due to the upward region adjacent to and on the low-mass side of the $M^*_{\mu\pi}$ bin. The cause of this region is not known: it can be seen from Fig. 5(I) that for $p_1/p_2 \sim 1$, as is required in a two-body apparatus, incorrect assignment of the preferred laboratory configuration ($p_\mu > p_\pi$) of decay (1) contributes $M_{\mu\pi}$ on the low-mass side and close to the $M^*_{\mu\pi}$ enhancement. It might be asked to what extent there could be contributions to this region by the systematics of particle assignment? In (b) the contributions from the reverse assignments of $(\mu,\pi)$ from $M^*_{\mu\pi}$ would be on the high-mass side of $M^*_{\mu\pi}$, and in Fig. 1 there would be contributions on each side of the $M^*_{\mu\pi}$ enhancement from low values of $p_1/p_2$. In the next section a pattern with $<10\%$ incorrect assignments of true $(\mu,\pi)$ will be shown; it has no corresponding features adjacent to $M^*_{\mu\pi}$.

Consideration of the shape of the indicated regions in (c) may raise two different types of questions: why do the statistically more significant data I give any indication at all of an upward fluctuation in the $M^*_{\mu\pi}$ bin, a lack of smoothness around $M^*_{\mu\pi}$ and resemblances with the patterns in Fig. 1? A reply that such patterns are found near 0.429 GeV, also, in other data with calibrated absolute mass scales must suffice until Sec. VI. A second question is then, why the pattern in (c) is not of still greater statistical significance: in these more prolific data should not $\chi^2_N$ scale directly with the ratio of the levels of the reference in the $M^*_{\mu\pi}$ bin in (c) and, say, in Fig. 1(b)? A complete reply requires further experimental studies in terms of the technicalities of particle identification, overall mass scale stability, resolution and, especially in terms of the experimental acceptances of the angular distributions of production and decay of $M^*_{\mu\pi}$. The preferred configuration of $p_\mu > p_\pi$ has been mentioned: the acceptance of the two-body experiments which requires $p_1 \sim p_2$ is, obviously, unfavorable for the preferred decay configuration. A preferred production configuration of $M^*_{\mu\pi}$ from $K^0_{\mu 3}$, which dominates the nature of patterns in experiments designed for the parallel configuration with $p_T = 0$ will now be considered.

Clark *et al.*[11] also reported that they found no evidence of $M^*_{\mu\pi}(0.429)$. Their experiment is similar to that of Bisi *et al.* in that it accepts the symmetrical configuration of $V^0$, but with still more stringent requirements of symmetry of the $(\pi,\pi)$ from $K_{\pi\pi}$, and $p_T \sim 0$. Only $V^0$ in which the components traverse two parallel detector systems with picture frame magnets, are recorded: Bisi *et al.* used a single magnet system which accepted larger values of $p_T$. Clark *et al.* show in a later report[6] of an experiment using the same apparatus, that in an $M_{\pi\pi}$ distribution of $\sim 5\times 10^4$ $K_{\pi\pi}$ events the full width at half height is 0.004 GeV and that the error in the mean absolute mass scale is $<0.002$ GeV. Their $M_{\mu\pi}$ distribution, in bins of 0.002 GeV has been converted to bins of 0.0025 GeV to give the difference histogram in Fig. 4(d). These data have been read from a larger diagram in a report; the reading errors are shown as in (c). For the indicated region, $\chi^2_{21} = 13.1$ (CLS=91%). In view of the demonstrated precision of the experimental technique, the resolution of a test pattern corresponding to that in Fig. 2 would be better than for the HBC. The observed degree of smoothness of (d) is inexplicable in terms of technicalities of calibration, or of particle assignment: it caused me to investigate the variation of the amplitude of the $M^*_{\mu\pi}$ enhancement with $p_T$ in the SC. There it is found that as well as the increase of significance of the $M^*_{\mu\pi}$ enhancement for the selection $p_\mu = p_1$, compared with $p_\pi = p_1$, there is also an increase[12,8] in significance for $p_T \sim p_T\text{max}$. In a data sample with $p_T \sim 0$, the $M^*_{\mu\pi}$ enhancement is insignificant. According to those studies the absence of an $M^*_{\mu\pi}$ enhancement in the observations of Clark *et al.* does not conflict with the presence of the enhancement in other experiments with $p_T > 0$. There is no immediately obvious pattern of lobes in Fig. 4(d), however a careful comparison with data I in (c), may raise a question about the possibility of correlations between this distribution with $p_T \sim 0$ and that of data I with $p_T \gtrsim 0$. One aspect will be considered now, and others in Sec. X and in the Appendix, section 3.

Statistical smoothness in terms of the usual $\chi^2$, e.g., in (a) and (d) in Fig. 4, does not signify the complete absence of correlations of the fluctuations with other data. In the Appendix, section 2, an obvious correlation between the fluctuations in (a) and (b) will be mentioned. Difference histograms from the combination of the data for (b), (c), and (d) are shown in Fig. 4; (e) is from the addition of the data of (c) and (d). For the indicated region $\chi^2_{21} = 35.7$ (CLS=2%), to be compared with $\chi^2_{21} = 40.9$ for (c). When the average of the references for (d), instead of the actual data, is combined with the actual data I, $\chi^2_{21} = 25.3$ (CLS=19%). Thus the addition of the observations of Clark *et al.*, which have 58% of the reference level in the $M^*_{\mu\pi}$ bin of those of data I, do not reduce markedly the $\chi^2$ of the pattern relative to that in data I, whereas the addition of the smooth reference reduces the $\chi^2$ as expected.

This result contrasts with the test in Fig. 3(d), where successive additions of the same distribution displaced in mass, obliterate the pattern. The observation of Clark *et al.* in the vicinity of $M^*_{\mu\pi}$ is not smooth with respect to that of data I in the usual sense of statistically smooth, i.e., random fluctuations. The addition of the data for (b), (c), and (d) is used for Fig. 4(f): $\chi^2_{21}=41.5$ (CLS $=3\times10^{-3}$), i.e., a slightly higher $\chi^2$ from more data than for (b), (e), or (d), and the pattern also resembles that of Fig. 1. The contents of the two obvious bins of the high-mass lobe are a fluctuation of 3.7 SD with respect to the average level of the reference there.

This type of compatibility of the data of the SC, Bisi *et al.*, and Clark *et al.* accentuates the question: How can there be any departure from physical smoothness in the vicinity of $M^*_{\mu\pi}$? The lobelike features in, e.g., (f) cannot be due to multimodal or otherwise ill-shapen mass resolution functions. Could they be due to some unexpected effect of incorrect assignment, or some other systematic experimental defect in $K^0_{\mu3}$ studies in both electronic detectors and bubble chambers?

## IV. COMPARISONS WITH $M^*_{\mu\pi}$ FROM $\nu$ INTERACTIONS

In $\nu$ beams with focused parents the antilepton contamination is low, so that in $\nu$ interactions producing only one possible $(\mu,\pi)$, as is the case for the data which will be used here, assignment of the appropriate charge to the $\mu$ causes $>90\%$ of true $(\mu,\pi)$ to be correctly assigned. Thus $M_{\mu\pi}$ distributions from bubble-chamber $\nu$ experiments are less affected by reverse assignments than $K^0_{\mu3}$ experiments; there are no quadratic ambiguities, the limitations in $p_1/p_2$ are less than with electronic detectors and $\mu$ and $\pi$ with momenta $>0.1$ GeV/$c$ moving at wide angles, or against the beam direction, are detected with high efficiency. Therefore, if the patterns near $M^*_{\mu\pi}$ were due to unexpected effects of reverse assignment of the true $(\mu,\pi)$, as distinct from incorrect assignment of other neutral combinations, lobes would not be seen in $\nu$ interactions. A relevant test about reverse assignments is in Fig. 9(I).

Figure 5(a) shows the $M_{\mu\pi}$ distribution in the vicinity of $M^*_{\mu\pi}$ from the data of Fig. 4(a) of paper (I), which is from $(\mu^-,\pi^+)$ and $(\mu^+,\pi^-)$. For convenience of comparison with other distributions, the calibrations made to the bin edges described in (I), have been applied here to the individual $M_{\mu\pi}$ before making the histogram, the error in the mean absolute mass scale is $<0.004$ GeV. For the indicated region and with respect to the fourth-degree polynomial: $\chi^2_{12}=20.9$ (CLS$=3\%$). Relatively more of the nonresonant background than the $M^*_{\mu\pi}$ enhancement can be removed[13] with the selection $p_1/p_2<2$; the statistical significance of the $M^*_{\mu\pi}$ decays is greater in (b): $\chi^2_{13}=33.2$ (CLS$=10^{-3}$). It can be argued that because of the observations of the $K^0_{\mu3}$ patterns, some such patterns could be expected in the indicated regions of Fig. 5 and, therefore, they should not be included in the data for the calculation of the polynomials. Such fourth-degree curves, calculated for the range $0.250<M_{\mu\pi}<0.550$ GeV, pass through the crosses. For (a) and for the fourth-, and

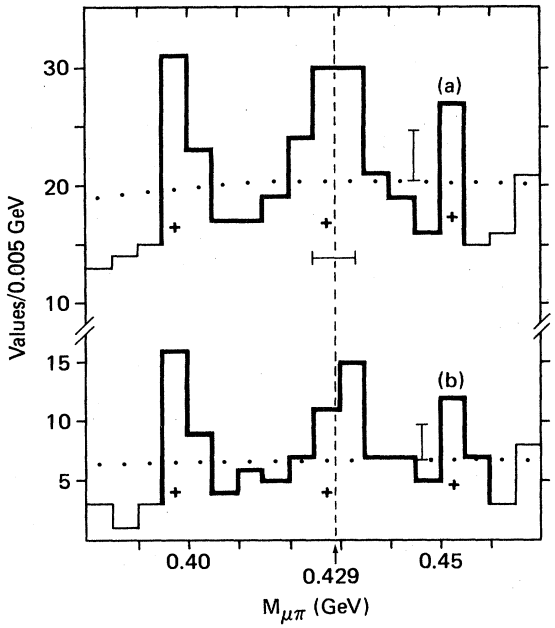


FIG. 5. Region of $M^*_{\mu\pi}$ from single $(\mu,\pi)$ combinations from $\nu$-nucleon interactions. Histogram (a) is from the total distribution from the HLBC and Gargamelle; (b) is selected with $p_1/p_2<2$. The fourth-degree polynomials calculated without the indicated regions pass through the crosses, the fifth- and sixth-degree polynomials pass between the crosses and the dotted reference. For the indicated regions of (a) and the fourth-, fifth-, and sixth-degree polynomials, $\chi^2_{12}=46.1$, 37.7, 32.5 (CLS$=3\times10^{-6}$, $9\times10^{-5}$, and $6\times10^{-4}$) respectively. Similarly, for (b). $\chi^2_{13}=100.2$, 81.8, and 68.2 (all CLS $<10^{-10}$). If considered as expected observations, because of the patterns in the preceding diagrams, the indicated fluctuations in (a) and (b) are unlikely to be due to statistical effects.

also fifth- and sixth-degree references which pass just above the crosses: $\chi^2_{12}=46.1$, 37.7, and 32.5 (CLS $=3\times10^{-6}$, $9\times10^{-5}$, and $6\times10^{-4}$, respectively; and for (b) similarly: $\chi^2_{13}=100.2$, 81.8, and 68.2 (CLS $\sim10^{-15}$, $10^{-12}$, and $10^{-9}$). The calculations for (b) are with small numbers of events, nevertheless they confirm an estimate with Poisson statistics that the probability is negligible that the patterns in the indicated region are statistical fluctuations. As in other distributions, the lobes are of statistical significance comparable to the $M^*_{\mu\pi}$ enhancement, e.g., the probability that an observation of a physically smooth distribution passing through the crosses in (a) would have a statistical fluctuation like the lower-mass lobe is $10^{-3}$, for the higher-mass lobe the probability is 5%, to be compared with $10^{-5}$ for the enhancement. For the same calculations with (b) these probabilities become $<10^{-5}$, $<10^{-5}$, $4\times10^{-3}$, respectively. Figure 6(c) shows the difference histogram from the data of Fig. 5(a), together with difference histograms from previous figures except (d), to be discussed shortly. The pattern in (c) is from single entries of $M_{\mu\pi}$; it has fewer indications than in the other patterns of subsidiary lobes in which there may be contributions from incorrect assignments. Other comparisons are in the caption to Fig. 6.

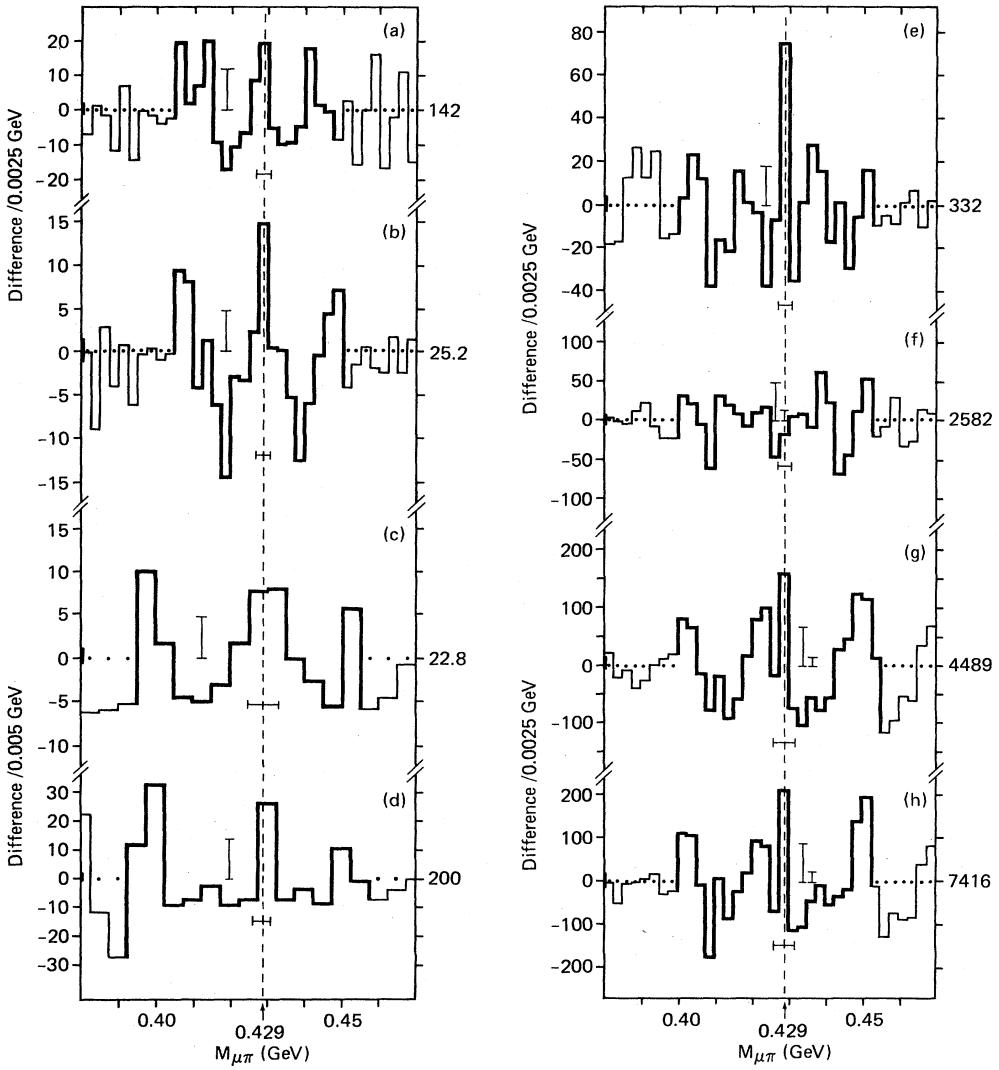


FIG. 6. Difference histograms of $M_{\mu\pi}$ distributions from $\nu$ interactions and six independent $K^0_{\mu 3}$ experiments; the ordinates are chosen to make 1 SD the same size in each diagram. Bubble-chamber experiments with different spectra of $(\mu,\pi)$ momentum: (a) HBC, both assignments as for Fig. 1(b), except $p_1/p_2<5$; (b) HLBC, both assignments as for Fig. 1(a), purest known sample of $V^0$ from $K^0_{\mu 3}$; (c) [from Fig. 5(a)] $\nu$ experiments, true $(\mu,\pi)$ are $>90\%$ correctly assigned; (d) hydrogen bubble chamber, $K^0_{\mu 3}\sim 0.5$ GeV/$c$, mostly both assignments (see text). The slightly varying locations of the lobelike features may be contrasted with the invariant location of the $M^*_{\mu\pi}$ fluctuations: the value $M^*_{\mu\pi}=0.429\pm 0.002$ GeV is determined from (a) and (b). Spark-chamber experiments with similar momentum spectra of $(\mu,\pi)$ but different acceptances of the configurations; (e) SC as for Fig. 3(b), $p_\mu=p_1$, probability $<10^{-5}$ that the enhancement is caused by a statistical fluctuation in the $M^*_{\mu\pi}$ bin, this observation confirms the value of $M^*_{\mu\pi}(0.429)$ from (a) and (b); (f) Clark *et al.* as for Fig. 4(d), $p_T\sim 0$; (g) from data I of Bisi *et al.* as for Fig. 4(c). A comparison of the fluctuations in (e), (f), and (g) makes clear why the pattern in (h) from the combination of their data is more significant statistically than the patterns in the individual diagrams. [A still more significant pattern from a combination of data I with data II is in Fig. 16(f): $\chi^2_{18}=62.1$ (CLS$=5\times 10^{-7}$).] If the four bubble-chamber observations and the observation from the combined spark-chamber data in (h) are considered together the probability is $\sim 10^{-10}$ that all the upward fluctuations at $M^*_{\mu\pi}$ are fortuitous. Similarly negligible probabilities obtain for the fortuitous occurrence of the symmetrically disposed low-mass and high-mass lobes.

Difference histogram (d) in Fig. 6 is from observations[14] of $V^0$ from monoenergetic $K^0_L\sim 0.5$ GeV/$c$ in a hydrogen bubble chamber, constrained to fit $K^0_{\mu 3}$. For the $V^0$ assigned as $(\pi,\pi)$ there is a feature in the $M_{\pi\pi}$ distribution which has half its amplitude in the range $0.495<M_{\pi\pi}<0.500$ GeV and which can be due to $K^0_S$. Therefore, the upward fluctuation which is augmented by the choice of bins shown (edges at 0.4275 and 0.4325 GeV, rather than at 0.425 and 0.430 GeV) can be due to $M^*_{\mu\pi}$; overall these data are statistically smooth; for the indicated region $\chi^2_{13}=10.8$ (CLS$=55\%$). If the indicated upward fluctuations are considered as the most conspicuous three such fluctuations in the range of the diagram the probability that, fortuitously, one of them should be

found in the $M^*_{\mu\pi}$ bin and two similarly located to lobes in the other diagram, is $<1\%$. It is difficult to study $M^*_{\mu\pi}$ from $K^0_{\mu 3}\sim 0.5$ GeV/$c$ because the favored configuration of the $M^*_{\mu\pi}$ c.m.s. with the $\mu$ in the forward hemisphere with respect to the line of flight, yields $p_\pi$ below the threshold for efficient detection. In a similar $K^0_{\mu 3}$ experiment of Cho *et al.*,[15] the $(\mu,\pi)$ were selected for $p_\pi > 0.075$ GeV/$c$. In the production[16] of the $K^0_L$, as well as the monoenergetic forward particles there are backward $K^0_L$ of momenta $\sim 0.08$ GeV/$c$ which do not enter the bubble chamber. If a suitable experiment could be devised, the $M^*_{\mu\pi}$ from those decays would be readily detectable, as can be inferred from Fig. 5(I). Cho *et al.* have not commented on $M^*_{\mu\pi}$.

In two of the three bubble-chamber $\nu$ experiments which yield $M_{\mu\pi}$ distributions in a relevant region, the $M^*_{\mu\pi}$ enhancement is not associated with comparable lobes. Histogram (a) in Fig. 7 shows the contributions to

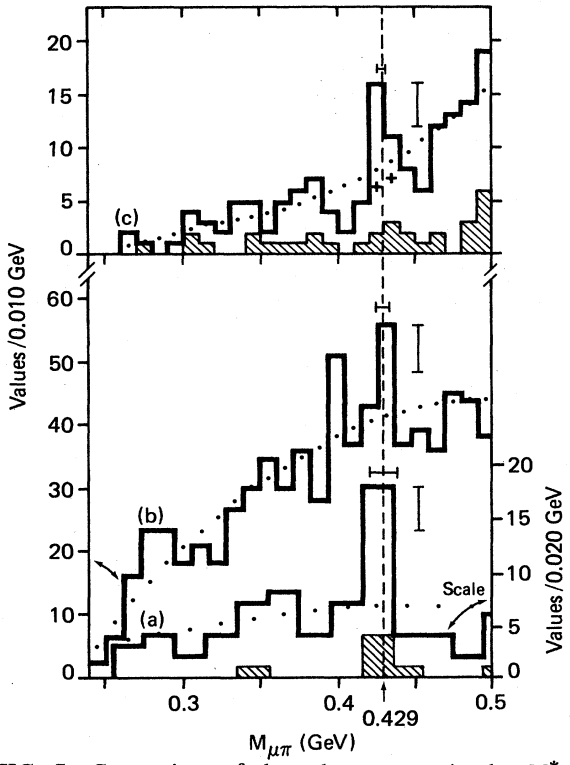


FIG. 7. Comparison of the enhancements in the $M^*_{\mu\pi}$ bin from three independent $\nu$ experiments. Histogram (a) is from the HLBC. This observation led to the study of the possible existence of $M^*_{\mu\pi}(0.429)$. Histogram (b) is from Gargamelle. Both (a) and (b) are shown with the bin locations of Fig. 2(I). The data are combined in this report in Fig. 5(a) which shows the gain in information from narrower bins. The 153 values of $M_{\mu\pi} < m_K$ in (c) are redrawn from Fig. 2 of Ballagh *et al.*, the solid line is the sum of the $(\mu^-,\pi^+)$ and $(\mu^+,\pi^-)$ contributions, the latter are shaded. [Those in (a) are also shaded, the more prolific $(\mu^+,\pi^-)$ of (b) are analyzed in (I).] According to any accepted understanding, the $M^*_{\mu\pi}$ distributions here and in the previous figure would be physically smooth. The probability is $<10^{-10}$ that statistical fluctuations in the histograms (a), (b), and (c), with independently calibrated mass scales, may cause the three enhancements which coincide in the $M^*_{\mu\pi}$ bins.

the data for Fig. 5 from $\nu$ experiments in propane in the 1.1-m$^3$ version of the HLBC; the $(\mu,\pi)$ are from events with only one possible neutral combination, classified by the scanners as "identified," i.e., as well as the assignment of the $(\mu,\pi)$ according to the appropriate charge for lepton conservation, there is a phenomenological indication of the $\mu$ and, especially of the $\pi^+$. The latter are commonly indistinguishable from protons $\gtrsim 1$ GeV/$c$. As a consequence of the selection the $\pi$ for (a) are mostly of low momenta, which is favorable for $M^*_{\mu\pi}$ detection; this was not realized when the analysis was made. The only $M_{\mu\pi}$ from $(\mu^+,\pi^-)$ within the range of the diagram, are shown hatched. It is from the enhancement in (a) that the study[2] of $M^*_{\mu\pi}$ arose: within the range of the indicated regions in Fig. 6, there are no lobes. Assuming that lobes of significance comparable to the enhancement might be expected, and taking note of the 0.020-GeV bin width, the probability is $\sim 10^{-3}$ that the lack of lobes with numbers of events similar to the $M^*_{\mu\pi}$ enhancement is due to a statistical fluctuation. Histogram (b) is from the $\nu$ and $\bar{\nu}$ experiments in propane and in freon in Gargamelle. The lobes in Fig. 5 are mostly contributed by these data, the smoothing by the misalignment between the lobes and the larger bins of Fig. 7(b) can be appreciated by comparing with the histogram in Fig. 5(a). For Fig. 7(b) the $(\mu,\pi)$ are selected from events with "one possible $\mu$" and one "possible $\pi$" of opposite charge. These different selection criteria from those for (a), cause any single neutral $(\mu,\mu)$ combinations to be included systematically in (b), of course incorrectly assigned as $(\mu,\pi)$. The considerable $(\mu^+,\pi^-)$ contribution to (b) is discussed in (I). Histograms (a) and (b) are shown in Fig. 7 according to the calibration of the bin edges in (I). The nominal bin width of 0.010 GeV in (b) is retained to facilitate comparison with histogram (c), which is from an experiment of Ballagh *et al.*,[17] who have searched for narrow enhancements in $M_{\mu\pi}$ distributions in the Fermilab 15-ft bubble chamber using a hydrogen-neon working fluid and a $\mu$ identifier, with energies of the $(\mu,\pi)$ combinations extending beyond 200 GeV.

There are 153 values in (c) for which $M_{\mu\pi} < m_K$, the maximum range relevant to a search for any phenomenon known to occur in $K^0$ decay. The histograms of Ballagh *et al.* can be read accurately; the error bar indicates the range of location of $M^*_{\mu\pi}$ (0.429) according to a mass-scale calibration from $K^0_S$. The contribution from $(\mu^+,\pi^-)$ is shown as for (a). The upward fluctuation in the $M^*_{\mu\pi}$ bin is described initially by Ballagh *et al.* as a 3-standard-deviation effect. Following the present procedures, for a fourth-degree polynomial, fitted over the range $0.250 < M_{\mu\pi} < 0.550$ GeV, and for the six bins in the range $0.400 < M_{\mu\pi} < 0.460$ GeV: $\chi^2{}_6 = 14.8$ (CLS$=2\%$). A similar reference, calculated without the 0.429-GeV bin, passes through the crosses: for the previous range $\chi^2{}_6 = 17.5$ (CLS$=4\times 10^{-3}$). The probability is $2\times 10^{-4}$ that the excess in the bin omitted is a statistical fluctuation which has occurred, specifically, in the $M^*_{\mu\pi}$ bin, rather than in any one of, say, ten neighboring bins in a physically smooth distribution represented by the polynomial through the crosses. For the three histograms in Fig. 7 considered together, the probability is $<10^{-10}$ that the

enhancements observed would all be statistical fluctuations, coinciding in the $M^*_{\mu\pi}$ bins of physically smooth distributions. The fluctuation in (c) is to be expected from the previous conclusions (I), which were reached without knowledge of the experiment of Ballagh *et al.*

It could be asked for Fig. 7, what features[18] would be expected in each of (a), (b), and (c) for the decay of a narrow $M^*_{\mu\pi}(0.429)$ state? In the difference histograms of Fig. 8, which are made directly from Fig. 7, the dotted curves superimposed on the enhancements in (a) and (b) represent the shape of observed distributions of $\Lambda^0$ and $K^0_S$, respectively, scaled for the decay of a particle of narrow width at 0.429 GeV. The appropriate background level for the placing of the curves is unknown; certainly, it is not the zero line because the polynomial is calculated with the region of the enhancement included, nor, for (c), is it as high as the level of the crosses in Fig. 7, because only one bin was omitted for their calculation. Placed as shown, the dotted curves in Fig. 8(a) and (b) appear compatible with the enhancement from a decay of a particle

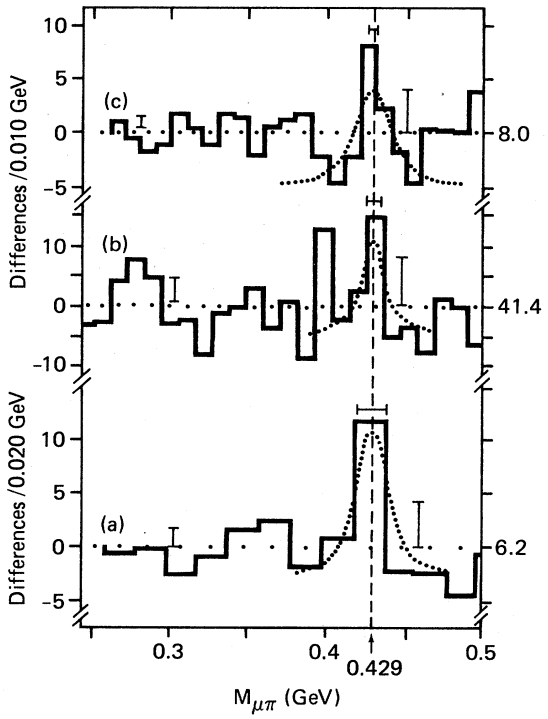


FIG. 8. Difference histograms obtained from Fig. 7: (a) for the HLBC, the dotted curve is scaled in mass from observed $\Lambda^0$ to a sharp decay at 0.429 GeV; (b) for Gargamelle, the dotted curve is scaled as for (a) from observed $K^0_S$, and (c) the dotted curve is scaled from the smooth line shape shown by Ballagh *et al.* for $K^0_S$ in their Fig. 4. The precise levels for the placing of the line shapes are unknown, the level of the zero line would not be correct because it is calculated with the enhancements included in the data. The $M^*_{\mu\pi}$ feature in each diagram appears compatible with the decay of a $(\mu,\pi)$ state of narrow width at 0.429 GeV. Most of the contributions to the lobes of Fig. 5(a) come from the data for (b). There are no similarly noticeable lobes in (a) or (c), where the selection of the combinations would reject most true $(\mu,\mu)$ combinations.

of narrow width at 0.429 GeV. The similarly placed dotted curve in (c) is scaled from the calculated resolution function for observed $K_{\pi\pi}$ decays in Fig. 4 of Ballagh *et al.* which peaks at $m_K$ and demonstrates that the error in the mean absolute $M_{\mu\pi}$ scale near 0.429 GeV is $<0.003$ GeV. The observed $M_{\pi\pi}$ distribution, in bins of 0.010 GeV, has a full width at half height of 4 bins, and the upper 25% of the amplitude is in one bin, similar to the observed mass-resolution functions of, e.g., data I and Clark *et al.* Following the considerations in Sec. II, in the region of 0.429 GeV in Fig. 8(c) the decay of a single narrow $(\mu,\pi)$ state can cause a feature with a peak in a single bin narrower than 0.010 GeV, with a full width at half height no greater than 0.033 GeV, which is the scaled observed width of the $K^0_{\pi\pi}$ feature. Within the limitations of the small number of events, the observation also appears compatible with the dotted curve for the decay of a narrow $(\mu,\pi)$ state of mass $0.429\pm0.002$ GeV. Ballagh *et al.* discuss their resolution function but they do not show, diagrammatically, how their expectations compare with the situation in (c); neither do they show the relationship of their observations to (a) and (b). They estimate that the amplitude of the fluctuation in (c) is compatible with the production rate of $M^*_{\mu\pi}$, reported in (I). Ballagh *et al.* conclude that they believe their observation in (c) is a statistical fluctuation, essentially because they consider it to be too narrow for the decay of a narrow $(\mu,\pi)$ state. They complete their findings with the sentence: "it would seem appropriate, nevertheless, for other experimenters to reexamine their $\mu\pi$ spectra."

This dilemma of Ballagh *et al.* is understandable. If an average reference of the weighted fitted polynomials of degrees 4, 5, 6, and 7, as described here for, e.g., Fig. 4, is used also for Fig. 2 of Ballagh *et al.*, the fluctuation in the bin $0.420<M_{\mu\pi}<0.430$ GeV is found to be the most significant, statistically, of all the upward fluctuations. This result is the same for their $(\mu^-,\pi^+)$ histogram and for the sum of the $(\mu^-,\pi^+)$ and $(\mu^+,\pi^-)$ histograms. The range of Fig. 2 of $0.25<M_{\mu\pi}<1.2$ GeV is the largest which Ballagh *et al.* show in 0.010-GeV bins. For the $(\mu^-,\pi^+)$ histogram there are three upward fluctuations $>2$ SD and for the sum of the $(\mu^-,\pi^+)$ and $(\mu^+,\pi^-)$ histograms there are two such fluctuations. None of these fluctuations, considered as isolated observations, is sufficiently significant to justify attention: unless Ballagh *et al.* refer their observations to a phenomenology of such distributions, they have no logical means of assigning a physical cause to any one of the fluctuations. This present phenomenology does not indicate that there are no other phenomena like the narrow $(\mu,\pi)$ state at 0.429 GeV; but it does identify the fluctuations at that mass in $M_{\mu\pi}$ distributions as a particular phenomenon. The observation of Ballagh *et al.* extends the range in visible energy of the $(\mu,\pi)$ combinations which produce such upward fluctuations, compatibly located within the limits of experimental error with the particular value of 0.429 GeV, from $<1$ GeV (Fig. 6) to $>200$ GeV (Fig. 7).

By a procedure analogous to that for Fig. 2(c), a pattern can be developed from the actual $M_{\pi\pi}$ observation in Fig. 4 of Ballagh *et al.* to test how a physical feature corresponding to that of the enhancement and lobes of Fig. 6(c)

would be seen in their experiment. Such a test shows that the expected pattern of Fig. 8(c) is an upward fluctuation essentially constant over some five bins and centered at $M^*_{\mu\pi}$. This pattern is not compatible with the observation; the probability is $<1\%$ that there are lobes around the $M^*_{\mu\pi}$ enhancement of Ballagh *et al.* as large as those in Fig. 6(c). That any lobes near the $M^*_{\mu\pi}$ enhancement in Figs. 8(a) and 8(c) are less than in, e.g., Fig. 6(c), is important to the model in Sec. VI which requires that lobes occur in $M_{\mu\pi}$ distributions in which there are incorrectly assigned $(\mu,\mu)$. Because of the $\mu$ identifier, the $M_{\mu\pi}$ distributions of Ballagh *et al.* might be expected to include fewer $(\mu,\mu)$, than distributions from the other $\nu$ experiments.

## V. TWO PHENOMENA

The experiments considered in this phenomenology are the only ones I know that conform to the criteria that their $M_{\mu\pi}$ distributions have been reported or made available in a format which allows some independent study of their smoothness, that they have a known calibration of the absolute mass scales and that they have a demonstrated ability to detect some known sharp decay. A synthesis of the observations from the nine experiments considered already, and one more in the Appendix, section 1 [Fig. 15(c)] shows that not only is there the phenomenon of the fluctuation from $M^*_{\mu\pi}(0.429)\rightarrow(\mu,\pi)$, but also a phenomenon of lobelike fluctuations in the vicinity of 0.429 GeV. The probability (e.g., $<10^{-10}$ for Fig. 6) that the collectivity of the lobelike fluctuations is a coincidence of statistical effects is negligible; they are not due to peculiarities of the mass measurements. Although the patterns in Figs. 17(c), 17(d), and 17(e) are compatible with the others, they are not included in this synthesis because of insufficient knowledge of their experimental circumstances.

The findings that there is no evidence for the existence of $M^*_{\mu\pi}(0.429)$ do not represent the actual physical situation revealed in the collectivity of independent experiments. It might be remarked, however, that each of the three findings mentioned here had justification in terms of the scientific method when reported: without more extensive comparative studies than were made by the groups of authors, the $M^*_{\mu\pi}$ phenomena could not have been identified at an acceptable confidence level.

For the purposes of the explanation of the lobes in the next sections, the following aspects are listed.

(i) In $M_{\mu\pi}$ distributions from nine of the ten experiments, upward fluctuations occur, which within the accuracy of calibration of their mass scales are compatible with an enhancement from a narrow $(\mu,\pi)$ state of mass $0.429\pm0.002$ GeV, already described in (I).

(ii) The absence of an upward fluctuation at $M^*_{\mu\pi}(0.429)$ with the selection $p_T\sim0$, in the observation of Clark *et al.*, does not conflict with the occurrence of such a fluctuation in the other experiments.

(iii) Fluctuations which can be attributed to lobes in the vicinity of $M^*_{\mu\pi}$ are observed in eight experiments, including that of Clark *et al.*

(iv) The ten experimental observations greatly restrict the possibility that the lobes are caused by errors in any one type of experiment.

(v) Because of the variation by $\sim0.020$ GeV in separation of the two major lobes [e.g., Figs. 6(a)—6(c)], compared with the invariant location of the enhancement from $M^*_{\mu\pi}\rightarrow(\mu,\pi)$, these lobes cannot be attributed to other narrow $(\mu,\pi)$ states.

However, the possibility that they might arise from a physical phenomenon different from decay (1) was viewed with lengthy circumspection: it is a fact that according to all accepted understanding, $M_{\mu\pi}$ distributions must be physically smooth over the range of the lobes and are so reported by experimenters.

## VI. A MODEL FOR LOBES

The variation in location could indicate that the lobes are due to a disintegration of $M^*_{\mu\pi}$ other than (1), with incorrect assignment of the products as $(\mu,\pi)$. That there is a higher- and a lower-mass lobe with a separation comparable to $E_\nu$ from $\pi\rightarrow(\mu,\nu)$, led to an extensive study of undetected $\pi$ decay in flight as a possible other type of "decay" of $M^*_{\mu\pi}$, which occurs to a certain extent in all the experiments. It seemed reasonable to conjecture that if an explanation were possible in terms of this mechanism, it would invoke only established principles: detailed analysis showed that such could not be the situation. There is no feasible means of simulating the comparable amplitudes of the lobes and the $M^*_{\mu\pi}$ enhancement over the range of decay lengths available in the various experiments (e.g., HBC$\sim10$ cm, Bisi *et al.* $\sim10$ m). Of particular physical importance is that only some narrow selections of the orientation of the $\pi$ decay with respect to the original $\mu$ from the $M^*_{\mu\pi}$ can cause lobes. This latter point, essentially that the lobes cannot be due to an isotropic daughter decay, made clear the kinematics of the only quantitatively tenable model which has been found.

It is based on the premise that as well as decay (1), there is another mode of disintegration via a short-lived particle with a mass near, but not at $m_\pi$, and which is produced by

$$M^*_{\mu\pi}\rightarrow(\mu^-,M^{*+}_{\mu\nu}) \tag{2}$$

and then decays

$$M^{*+}_{\mu\nu}\rightarrow(\mu^+,\nu)\ . \tag{3}$$

Since there is evidence also for the decay of $\overline{M}^*_{\mu\pi}$ via $\overline{M}^*_{\mu\nu}$, the muons will be indicated by $(\mu_1,\mu_2)$ such that

$$M^*_{\mu\pi}\rightarrow(\mu_1,M^*_{\mu\nu}) \text{ and } M^*_{\mu\nu}\rightarrow(\mu_2,\nu)\ .$$

Here $\mu_1$ has the same lepton number as $M^*_{\mu\pi}$ and $\mu_2$ the opposite.

The proposed disintegration is not a three-body decay of $M^*_{\mu\pi}$, but if (2) and (3) are in rapid succession the overall result

$$M^*_{\mu\pi}\rightarrow(\mu_1,\mu_2,\nu) \tag{4}$$

appears qualitatively as such. In a true three-body decay the $M_{\mu\mu}$ could be expected to be a smooth distribution. However, the $M_{\mu\mu}$ from (2) and (3) can form lobes, provided there is a tendency in the $M^*_{\mu\nu}$ c.m.s. for the momentum $\mathbf{p}^*_2$ of $\mu_2$ to be aligned with $\mathbf{p}^*_1$ of $\mu_1$. Exam-

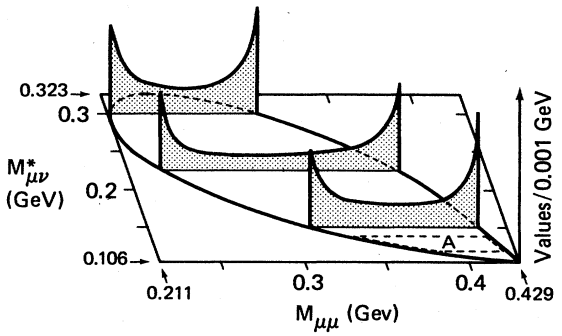


FIG. 9. Examples of calculated $M_{\mu\mu}$ distributions from the decays: $M^*_{\mu\pi}\to(\mu_1,M^*_{\mu\nu})\to(\mu_1,\mu_2,\nu)$ for various sharp values of $M^*_{\mu\nu}$. The model is concerned with the region A.

ples of $M_{\mu\mu}$ calculated from $M^*_{\mu\pi}(0.429)$ and for narrow values of $M^*_{\mu\nu}$ are shown in Fig. 9. For illustrating the effect of alignment, the particular weighting is not critical: here, the integrated decay probability of $M^*_{\mu\nu}$ in its c.m.s. is constant with $\theta$, the inclination of $\mathbf{p}^*_2$ to $\mathbf{p}^*_1$. The angle $\theta$ is inset in Fig. 10, which shows relationships between $M_{\mu\mu}$ and $\cos\theta$ for $M^*_{\mu\nu}=0.125$ GeV, a value for which the lobes have spacings similar to those in the $M_{\mu\mu}$ assignment of the combinations for Fig. 5. $M'_{\mu\mu}$ from incorrect $(\mu,\mu)$ assignment of the $(\mu,\pi)$ from decay (1) are shown also; the distributions of the $M'_{\mu\mu}$ on each side of $\cos\theta^*=0$ in Fig. 10 will be used in identifying and isolating the observed $M'_{\mu\mu}$.

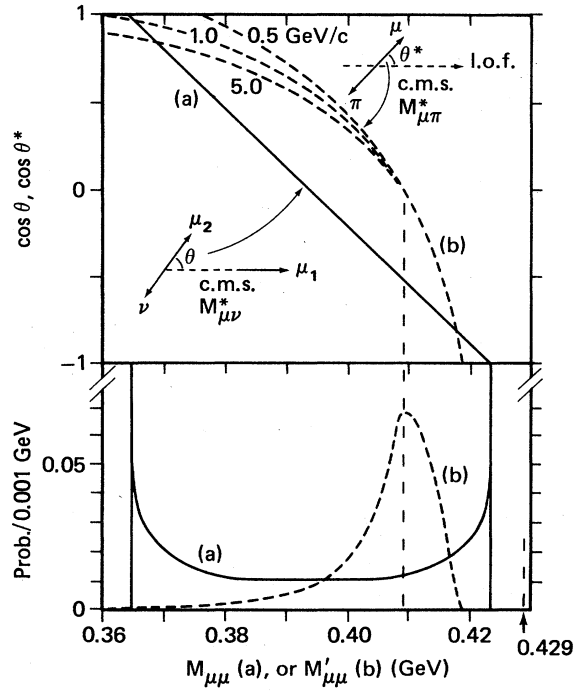


FIG. 10. Observed masses vs angular distribution in the decays of $M^*_{\mu\pi}(0.429)$ and $M^*_{\mu\nu}$ of 0.125 GeV. Curves (a) show the dependence of the observed $M_{\mu\mu}$ (lower diagram) from $M^*_{\mu\pi}\to(\mu_1,M^*_{\mu\nu})\to(\mu_1,\mu_2,\nu)$, with $\theta^*$, inset in upper diagram. Curves (b) show the dependence of $M'_{\mu\mu}$ from incorrectly assigned $M^*_{\mu\pi}\to(\mu,\pi)$ with $\theta^*$. Three values of $P$ are shown in the upper diagram. The curve in the lower diagram is for $P=1.0$ GeV/$c$, which is representative of the range $0.5<P<5$ GeV/$c$.

$M'_{\mu\pi}$ from the "$(\mu,\pi)$" assignment of the $(\mu,\mu)$ from decays (2) and (3) can occur on either side of $M^*_{\mu\pi}$. The $M'_{\mu\pi}$ distribution in Fig. 11(b) is from a smoothed Monte Carlo calculation of the $p_\mu=p_1$ assignment of $(\mu,\mu)$ when $M^*_{\mu\nu}=0.127$ GeV. It has been assumed that for the $K^0_L$ decays the direction of the normal to the decay plane in the $M^*_{\mu\pi}$ c.m.s. is isotropic relative to the LOF and that, typically, $P=1$ GeV/$c$. For comparison, (a) shows the difference histogram from the HBC distribution in Fig.

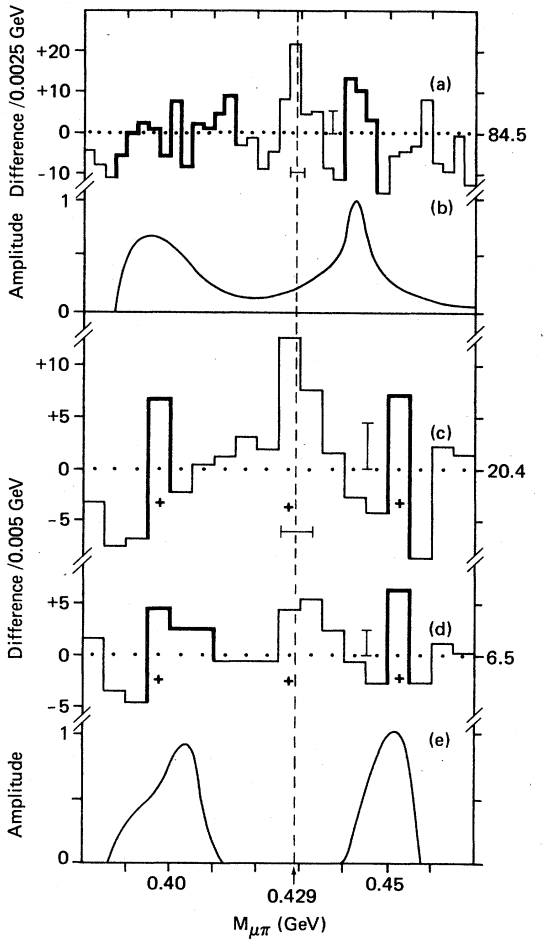


FIG. 11. Calculated $M'_{\mu\pi}$ for the $p_\mu=p_1$ selection of $(\mu,\mu)$ from the decay: $M^*_{\mu\pi}\to(\mu_1,M^*_{\mu\nu})\to(\mu_1,\mu_2,\nu)$ compared with observed $M_{\mu\pi}$ from $K^0_{\mu3}$ decays and $\nu$ interactions. The observed difference histogram from the fourth-degree polynomial for the HBC is in (a); (b) shows the calculated $M'_{\mu\pi}$ with no preferred alignment of the plane of decay of $M^*_{\mu\pi}$ relative to the LOF. For convenience of comparison, the data from $\nu$ interactions in Fig. 5(a) have been assigned $p_\mu=p_1$, independently of the original assignments: (c) observed difference histogram from the fourth-degree polynomial, all data; (d) selection of $p_1/p_2<2$; (e) $M'_{\mu\pi}$ calculated similarly to (b), except that the normal to the plane of decay of $M^*_{\mu\pi}$ has been taken as preferentially inclined to the LOF. In both (b) and (e) the simulated lobes resemble the observations in location and shape.

3(c), which is chosen because there are no effects from a beam pipe. Other information is in the caption. The position of the lobes in Fig. 5 cannot be simulated by using the decay plane orientation for Fig. 11(b). For the calculation of (e), the decay plane is inclined so that $p^*_{\mu_1}$ is, preferentially, in the forward hemisphere relative to the LOF of $M^*_{\mu\pi}$. Simulation of the lobes in (a), (c), and (d) is only feasible in the range $0.120 \lesssim M^*_{\mu\nu} \lesssim 0.130$ GeV. The lobe spacing for $P \sim 50$ GeV/$c$, which is appropriate to the data of Ballagh *et al.*, is approximately the same as in (e). Thus the test for the appearance of such lobes in their $M_{\mu\pi}$ distributions, described in Sec. IV, is meaningful.

Calculations such as these show that the model is able to produce the differing appearances of lobes in, e.g., Figs. 6(a)—6(d) and to indicate possible, but not necessarily unique kinematical causes of shapes and locations. In Sec. VIII the mass of $M^*_{\mu\nu}$ will be determined directly from the selected $(\mu,\pi)$, assigned as $(\mu,\mu)$. Any true $M_{\mu\mu}$ will be invariant and, specifically, unaffected by the orientation of the c.m.s. of $M^*_{\mu\pi}$: the shape of the $M_{\mu\mu}$ distribution depends directly on the properties of $M^*_{\mu\nu}$.

## VII. ARE THERE $(\mu,\mu)$ IN THE "$(\mu,\pi)$"?

In the experiments which produced the distributions of Figs. 1 to 6 it cannot be proved that the small fraction ($< 10\%$) of combinations causing the lobes are $(\mu,\pi)$ rather than $(\mu,\mu)$. In $\nu$ experiments $(\mu,\mu)$ are observed: in 4000 interactions in a spark chamber[19] in the same experiment as the HLBC, there were 33 possible $(\mu,\mu)$ where both particles traversed $> 30$ cm of iron. If all of the 443 combinations in the total $\nu$ data which can yield $M_{\mu\mu}$ in the range of Fig. 12 were actually $(\mu,\mu)$, which is certainly not the case, only 80 would have had both momenta above the threshold for $\mu$ identification in the spark chamber. The observations from the spark chamber did not yield a $M_{\mu\mu}$ distribution; however, they set a lower limit to overall $(\mu,\mu)$ production and are compatible with the assumptions of the model. In particular, 29 of the 33 possible $(\mu,\mu)$ combinations are $p_{\mu-} > p_{\mu+}$, i.e., $p_{\mu_1} > p_{\mu_2}$: almost all $(\mu,\mu)$ from the model have $p_{\mu_1} > p_{\mu_2}$.

There are no lobes in Figs. 7 and 8 comparable to the $M^*_{\mu\pi}$ enhancements in the two $\nu$ experiments where the efficiency of $(\mu,\pi)$ selection is expected to be high. A similar indication comes from the 240 combinations from the X4 data in which one of the tracks shows a nuclear scatter. This selection practically excludes $(\mu,\mu)$: the $M^*_{\mu\pi}$ enhancement is not accompanied by significant lobes in this subset of the data. A complementary indication is from $K^0_{\mu 3}$ combinations with noninteracting tracks[20] shown in Fig. 15(c). The selection favors $(\mu,\mu)$ with respect to $(\mu,\pi)$: the distribution is correlated with the observations from the HBC but the $M^*_{\mu\pi}$ enhancement is less significant with respect to the lobes than in either the HBC or HLBC. While none of these observations, individually, has sufficient statistical significance to prove that the lobes are caused by $(\mu,\mu)$, the probability is $< 10^{-5}$ that their collective compatibility is fortuitous.

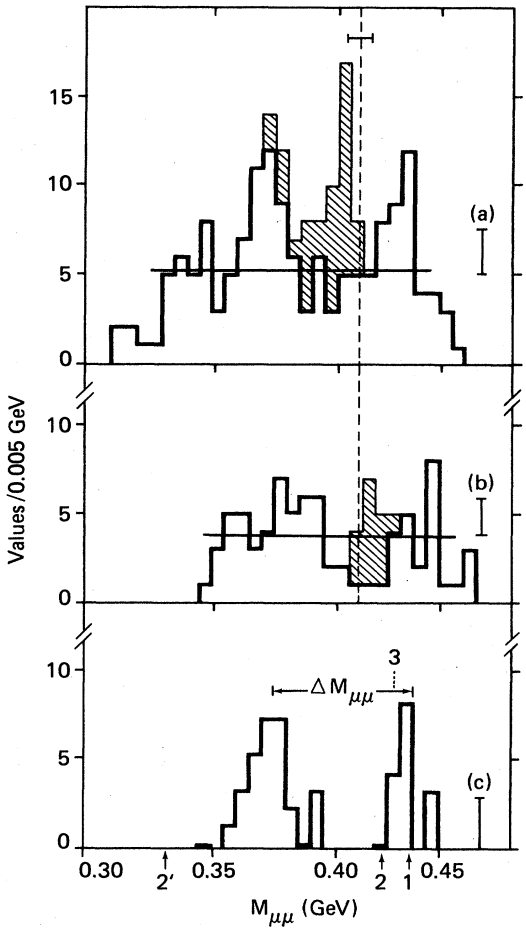


FIG. 12. Histograms of $M_{\mu\mu}$ from the $(\mu,\pi)$ for Fig. 5(a) assigned as $(\mu,\mu)$, in nonoverlapping samples: (a) is for combinations for which, originally $1 < p_\mu/p_\pi < 4$; (b) is for $1 < p_\pi/p_\mu < 4$. The hatched regions are from the combinations which give $M_{\mu\pi}$ in the range $0.425 < M_{\mu\pi} < 0.435$ GeV, which includes most of the $M^*_{\mu\pi}$ enhancement in Fig. 5; the distribution of these $M_{\mu\mu}$ about the dotted vertical line is as calculated for $M^*_{\mu\pi} \to (\mu,\pi)$ in (b) in the lower part of Fig. 10. After removal of the hatched regions and the background below the horizontal line, as described in the text, the remaining distribution from (a) and (b) is shown in (c). This contains the $M_{\mu\mu}$ from $M^*_{\mu\pi} \to (\mu_1 + M^*_{\mu\nu}) \to (\mu_1,\mu_2,\nu)$. The arrow at 1 indicates the only possible value of $M_{\mu\mu}$ if $M^*_{\mu\nu} = m_\mu$; positions 2 and 2' are for the extreme $M_{\mu\mu}$ if $M^*_{\mu\nu} = m_\pi$; $\Delta M_{\mu\mu}$ is the separation between the means of the observed values, considered as two groups. Position 3 is the maximum $M_{\mu\mu}$ to be expected from the indicated $\Delta M_{\mu\mu}$.

## VIII. LOBES FROM $\nu$ EXPERIMENTS

For a determination of the value of $M^*_{\mu\nu}$ it is desirable to separate most products of decay (1) from the $(\mu,\mu)$ candidates. This requires the best possible accuracy in assignment of the true $(\mu,\pi)$ from $M^*_{\mu\pi}$ and, therefore, only the $\nu$ data of Fig. 5 will be considered. Histogram (a) in Fig. 12 is the $M_{\mu\mu}$ distribution calculated from the reassignment of all $(\mu,\pi)$ within the range of Fig. 5, i.e.,

$0.380 < M_{\mu\pi} < 0.470$ GeV, and with $1 < p_\mu/p_\pi < 4$. The reason for this selection will become apparent, shortly. The hatched region is from the range $0.425 < M_{\mu\pi} < 0.435$ GeV, which includes most of the $M^*_{\mu\pi}$ enhancement. The dashed ordinate is located as in Fig. 10, being the calculated upper limit of $M'_{\mu\mu}$ from $M^*_{\mu\pi}$ for $p_\mu = p_1$. Histogram (b) is for $1 < p_\pi/p_\mu < 4$, with procedure otherwise identical with (a): here the same dashed ordinate is the calculated lower limit of $M'_{\mu\mu}$ from $M^*_{\mu\pi}$ for $p_\pi = p_1$; the distribution of these $M'_{\mu\mu}$ in (a) and (b) is compatible with that in Fig. 10. In Fig. 5 the polynomials are, essentially, at a constant level over the range of the diagram. An estimate of the background of processes not related to $M^*_{\mu\pi}$ is obtained from the fourth-degree polynomial discussed for that figure and which passes through the crosses. In order to set a level in Fig. 12 for the background of unrelated processes, the horizontal lines are placed so that the parts of the histograms below them have the same numbers of values as are below the polynomial through the crosses in Fig. 5. After removal of the hatched regions above the lines the remaining regions in (a) and (b) above the lines are estimates of the $M_{\mu\mu}$ distribution associated with the lobes in the corresponding $M_{\mu\pi}$ distribution. These are combined in histogram (c) for which, evidently, $p_1/p_2 < 4$.

A first estimate of the value of $M^*_{\mu\nu}$ can be derived from $\Delta M_{\mu\mu}$, the separation between the mean masses of the higher and lower lobes. The arrows show extreme $M_{\mu\mu}$ for ideal measurements of different $M^*_{\mu\nu}$ of narrow mass. If $M^*_{\mu\nu} = m_\mu$, there is only one value: $M_{\mu\mu} = 0.429$ GeV, located at 1; for $M^*_{\mu\nu} = m_\pi$, the extremes are at 2 and 2′. In this region $d(\Delta M_{\mu\mu})/dM^*_{\mu\nu} \sim 2$. For the $\Delta M_{\mu\mu}$ shown, $M^*_{\mu\nu} = 0.125$ GeV; the highest $M_{\mu\mu}$ should have occurred at 3. The discrepancy (0.006 GeV) with the weighted mean of the upper group of values is within the errors of calibration of the $M_{\mu\mu}$ scale (0.005 GeV) and the mass of $M^*_{\mu\pi}$ (0.002 GeV). It can be inferred from Fig. 9 that if $M^*_{\mu\nu}$ were sufficiently narrow, the lobes in Fig. 12(c) would have similar widths but not, necessarily, similar amplitudes: qualitatively, they are not of equal width.

The ratio $p_1/p_2 < 4$ was chosen by inspection because it is the maximum at which extension of the range of $M_{\mu\pi}$ of the combinations does not add to the distribution in (c). The histogram in Fig. 13 is obtained by the same method as in Fig. 12(c), except that $p_1/p_2 < 5$. The hatched regions are the contributions which appear if the range in $M_{\mu\pi}$ of the combinations is extended to 0.490 GeV: extension below 0.380 GeV would contribute two values at the extreme left. As can be inferred from Fig. 10, without restrictions on the ranges of $M_{\mu\pi}$ and $p_1/p_2$, the spreading of $M_{\mu\mu}$ from the true $(\mu,\pi)$ reduces the significance of the lobes. In essence, the value of $M^*_{\mu\nu}$ can be determined by calculating lobes which coincide with the observed lobes and which have, therefore, the same $\Delta M_{\mu\mu}$. The distribution of fits between the observed distribution of Fig. 13 and calculated distributions for various $M^*_{\mu\nu}$ and widths is shown in Fig. 14. Good fits are obtained for $M^*_{\mu\nu} \sim 0.127$ GeV and a width of 0.005 GeV, the cross corresponds with the calculated curve in Fig. 13. Such a level of best fit is obtained when the calculated curve is allowed freedom of displacement relative to the histogram:

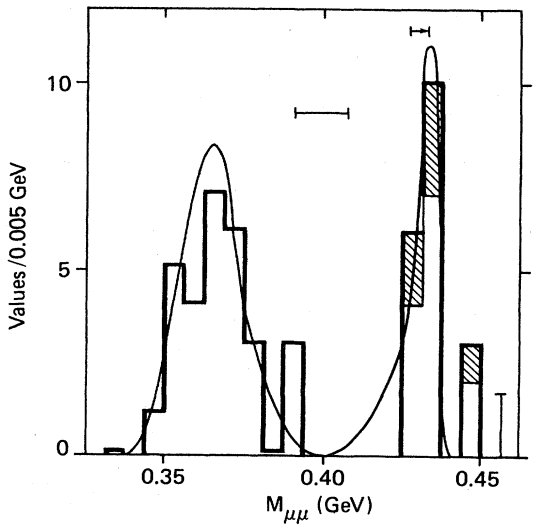


FIG. 13. Observed and simulated $M_{\mu\mu}$ distributions. The histogram is the observed distribution obtained by the same procedure as in Fig. 12(c), except $p_1/p_2 < 5$. The hatched values are contributed by extending the range of the $M_{\mu\pi}$ of the combinations to 0.490 GeV. The curve is the calculated distribution for $M^*_{\mu\nu} = 0.127$ GeV and width 0.005 GeV; in order to produce the best fit it has been displaced, bodily, in absolute mass as shown by the arrow near the right-hand peak. The horizontal error bar represents the combined errors in the absolute mass scale and in the value of $M^*_{\mu\pi}$.

the arrow shows the actual displacement (0.005 GeV), which is less than the possible errors of calibration. The $> 90\%$ fits occur with the same displacement, which has been maintained for the remainder of Fig. 14. The fitting procedure discards calculated values which are outside the range of the calculated curves, therefore it is quantitatively significant only for the identification of the best fits. Limits imposed by consideration of experimental resolution are shown by the dashed rectangle.

For the calculated curves for Fig. 14 the probability of decay of $M^*_{\mu\nu}$ has been weighted, empirically, by $(1 + 0.33\cos\theta)\cos^2\theta$. While similar values of $M^*_{\mu\nu}$ and its width are obtained by other procedures, the determination of the specific angular distributions of the decays depends on the background level and also on the observed range of $p_1/p_2$. The present data are inadequate to establish, independently, the angular distributions of decays (2) and (3): they indicate, of course, that the decays are strongly aligned.

Approximate relative production and decay rates of $M^*_{\mu\pi}$ can be deduced from analyses of the type of Figs. 12 and 13, and from consideration of other diagrams. If $R_1(\text{sec}^{-1})$ is the rate of decay of $M^*_{\mu\pi}$ via $(\mu,\pi)$ and $R_2$ the rate via $M^*_{\mu\nu}$, then the range $2.5 < R_2/R_1 < 5$ is estimated to accommodate the decays of $M^*_{\mu\pi}$ from the $K^0_{\mu 3}$ and $\nu$ experiments, and the uncertainty of the shape of the background distribution. From the $K^0_{\mu 3}$ data of Fig. 1 the production of $M^*_{\mu\pi}$, expressed as a fraction $(F)$ of all $M_{\mu\pi}$ is $1 < F < 3\%$. The distribution of Fig. 3(c) has not been

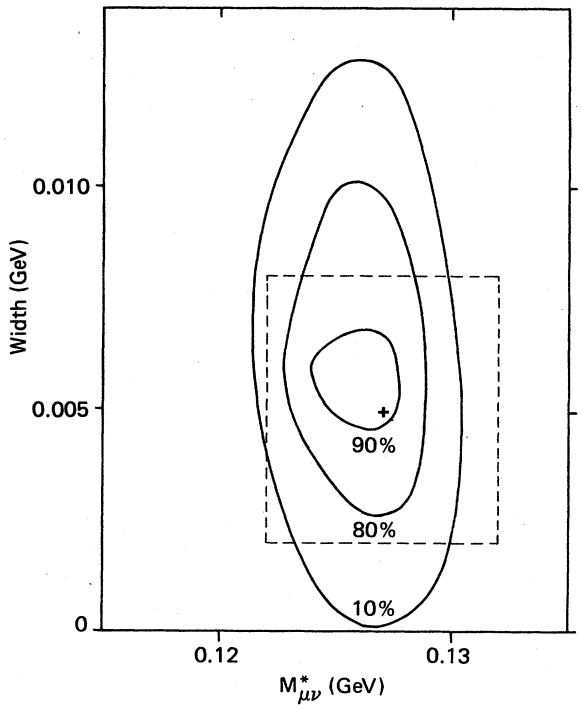


FIG. 14. Fits of calculated distributions to the observed histogram in Fig. 13; the parameters for the calculated curve shown in that figure are indicated by the cross. The bounds to the range of experimentally possible fits, determined from the observations and shown by the dashed line are $M^*_{\mu\nu}=0.127\pm0.005$ GeV; width $0.005\pm0.003$ GeV.

used: although its correction procedure is able to reveal the location in mean absolute mass of features of the distribution, a full amplitude of structure, such as in Fig. 1, cannot be obtained. Ballagh *et al.* consider that their enhancement [Fig. 7(c)] indicates a rate compatible with (I). If $F$ is restricted to $M_{\mu\pi}<m_{K'}$ the range $5<F<15\%$ accommodates the $\nu$ experiments. Precise determinations of $R_2/R_1$ and $F$ will require more experimental information on the background distribution of $M_{\mu\pi}$.

## IX. ESSENTIALS OF THE MODEL

In this determination of the mass of $M^*_{\mu\nu}$ it is assumed that (i) $M^*_{\mu\pi}$ is of mass 0.429 GeV and of narrow width, (ii) $\mathbf{p}^*_{\mu_2}$ tends to be aligned with $\mathbf{p}^*_{\mu_1}$ in the $M^*_{\mu\nu}$ c.m.s., (iii) the cause of the lower mass lobe being the wider is the width of $M^*_{\mu\nu}$, and (iv) the spatial separation of decays (2) and (3) is $<1$ mm.

As discussed earlier the mass of $M^*_{\mu\pi}(0.429)$ was determined in the $K^0_L$ experiments of Fig. 1 and confirmed relative to $K^0_{\pi3}$ in the SC (e.g., in Fig. 3); importantly, in Fig. 7 (and in all other diagrams), the absolute mass scales were calibrated without any reference to $M^*_{\mu\pi}$. For the range of values which could be of any possible relevance to the lobes, say, $0.115<M^*_{\mu\nu}<0.135$ GeV, the calculated mass of the upper lobe is $0.419<M_{\mu\mu}<0.425$ GeV. Taking account of the calibration errors, the upper lobe is to be expected in the range $0.413<M_{\mu\mu}<0.431$ GeV. The weighted mean mass of the upper lobe in Fig. 13 is, numerically, 0.4257 or 0.4275, depending on whether only the values in the higher-mass lobe of the calculated curve, or all of the group at higher mass are considered. Both these results are within the expected range.

Alignment of $\mathbf{p}^*_{\mu_2}$ with $\mathbf{p}_{\mu_1}$ is the cause of the lobes. For the relevant range of $M^*_{\mu\nu}$, it is an intrinsic requirement of the model that the spread in $M_{\mu\mu}$ of the upper-mass lobe, as distinct from its amplitude, must be smaller, or at most equal to that in the lower. Simulation of the unequal spreads is optimum for a width of $M^*_{\mu\nu}$ of $0.005\pm0.003$ GeV: the error includes effects of various postulates for the angular distribution in decays (2) and (3). An upper limit to the lifetime and, implicitly, a lower limit to the width of $M^*_{\mu\nu}$ can be set independently. Had the combined flight paths of $M^*_{\mu\pi}$ and $M^*_{\mu\nu}$ been $\geq1$ mm, the gap between the $\nu$-interaction vertex and the origin of $\mu_1$ or $\mu_2$ would have been observable. The possibility of any gaps due to lifetimes was investigated throughout the $\nu$ experiments (I): no observation required interpretation as a possible flight path. This finding sets an upper limit to the lifetime of the cascades (2) and (3) of $<10^{-12}$ sec.

Calculations of the type for Fig. 13 simulate the lobes effectively; no other feasible explanation of lobes has been found.

## X. OTHER POSSIBLE CONNECTIONS

According to the model the transverse momenta of $(\mu,\mu)$ from decays (2) and (3) can exceed the maximum value of the transverse momentum of the $(\mu,\pi)$ from $K^0_{\mu3}\rightarrow(M^*_{\mu\pi},\nu)$. This fact may be related to the finding (Sec. III) that structure in the $M_{\mu\pi}$ distributions without $(\mu,\pi)$ identification is most pronounced at high values of $p_T$: the $(\mu,\mu)$ which, incorrectly assigned, produce the lobes can have a higher $p_T$ than the true $(\mu,\pi)$ with corresponding values of $M_{\mu\pi}$. Thus fitting procedures constrained to $K^0_{\mu3}$ decays, as have been used for (d) and (g) in Fig. 6 might not accept all possible $V^0$ from $M^*_{\mu\pi}$.

It is possible that $M^*_{\mu\pi}(0.429)$ is produced in $\mu$ interactions with nucleons. If the process $\mu^-+p\rightarrow M^*_{\mu\pi}+n$ exists, decays (2) and (3) might be detected in neutral-dimuon invariant-mass distributions. It can be seen from Figs. 12 and 13 that the larger contribution to the $M_{\mu\mu}$ distribution from $M^*_{\mu\pi}$ decay would be due to the lower-mass lobe and, therefore, in the range $0.35<M_{\mu\mu}<0.40$ GeV. In a study of interactions of 10.5-GeV/$c$ $\mu^-$ in a lead-glass target,[21] Le Britton *et al.* determined various $d\sigma/dM_{\mu\mu}$ in steps of 0.05 GeV in $M_{\mu\mu}$. The observed cross section relevant to decays (2) and (3) is decreasing rapidly near 0.40 GeV; Le Britton *et al.* show that most, if not all of the $M_{\mu\mu}$ distribution is due to known processes. They contemplate the production of a heavy neutral lepton $M^0\rightarrow(\mu,\mu,\nu)$ as a contributor to the dimuon production and conclude that it is unlikely to account for $>10\%$ of the events; their neutral-dimuon-mass distribution has no aspect which excludes the possibility of some contribution from decays (2) and (3).

Badier *et al.* have studied a prolific spectrum of neutral dimuons with large $p_T$, produced by 150 GeV/$c$ $\pi^-$ in a beam dump experiment: their $M_{\mu\mu}$ distribution[22] is in agreement with their expectations from the decay of $\rho,\omega,\phi$ resonances, and indicates that the errors in the

mean absolute scale are $<0.02$ GeV. The dimuon-mass distribution from decays (2) and (3) would be expected in a region which is almost clear of any effects of the resonances. If the $M_{\mu\mu}$ distribution in Fig. 1 of Badier *et al.* is replotted in Fig. 13, some of the largest fluctuations about their background curve are found to be similarly placed to the lobes. The stated mass resolution of 0.12 GeV of Badier *et al.* allows no conclusion other than the similarity is a statistical coincidence with a probability of occurrence of $<10^{-4}$. This situation seems to merit further study. None of the indications is incompatible with the existence of decays (2) and (3) which might arise through the production of $M^*_{\mu\pi}(0.429)$: lepton conservation would require such production to be of the types $\pi^-+p\rightarrow M^*_{\mu\pi}+\bar{\nu}_\mu+n$, $\pi^-+p\rightarrow M^*_{\mu\pi}+\bar{M}^*_{\mu\pi}+n$, etc.

Although the aim of this report is to explain the lobes, it has become clear that the observational properties of $M^*_{\mu\nu}$ are similar to some of those of $W^\pm$ as described by Lee and Yang.[23] In the CERN series of $\nu$ experiments at the 28-GeV proton synchrotron, which provided the present $\nu$ data, searches for $W^+$ were planned with the assumption that $\mu^+$ from $W^+\rightarrow(\mu^+,\nu)$ would have higher momenta than $\mu^-$ from $\nu+N\rightarrow\mu^-+N'+\cdots$. In the $\nu$ spark-chamber experiment (Sec. VII) there were no significant occurrences of $p_{\mu^+}>p_{\mu^-}$. The results are compatible with the predominance of $p_{\mu_1}>p_{\mu_2}$ in the decay of $M^*_{\mu\nu}$.

It might be conjectured how neutral particles with mass similar to $M^*_{\mu\nu}$ and with properties like some of those[24] of $W^0$ appear in such experiments? In the $M_{\mu\gamma}$ distributions of Fig. 12(I), which were obtained from muon–single-$\gamma$ combinations, there is an enhancement considered[25] due to

$$M^*_{\mu\gamma}(0.429)\rightarrow(\mu,\gamma)\ . \tag{1'}$$

In analogy with decays (2) and (3), is there also a decay

$$M^*_{\mu\gamma}\rightarrow(\mu,M^*_{\gamma\gamma})\ , \tag{2'}$$

followed by

$$M^*_{\gamma\gamma}\rightarrow(\gamma,\gamma) \tag{3'}$$

in which there is some alignment of $\mu$ and $\gamma$?

For a mass of $M^*_{\gamma\gamma}$ similar to $M^*_{\mu\nu}$, the decay (3′) would be difficult to separate from the commonly observed $\pi^0\rightarrow(\gamma,\gamma)$. Even if it occurred with the rate of the true $\pi^0$ decay, it could not be identified without a specialized search. If there were some alignment of $\mu$ and $\gamma$ in (2′) and (3′), analogous to that of $(\mu_1,\mu_2)$ in (2) and (3), and one of the $\gamma$ escaped detection, lobes could be produced in $M_{\mu\gamma}$ distributions by the $(\mu,\gamma)$ combinations of (2′) and (3′). Because $m_\gamma=0$ and no incorrectly assigned particle would be involved, the lobes calculated by analogy with those in Fig. 3(a) are both on the low-mass side of $M^*_{\mu\gamma}$; one almost contiguous with $M^*_{\mu\gamma}$, the other near $m_\mu$. The $(\mu,\gamma)$ observations giving Fig. 12(I), and also the $(\mu,\gamma,\gamma)$ can be searched in these terms.

## XI. CONCLUSION

It was shown previously that the probability that the $M^*_{\mu\pi}\rightarrow(\mu,\pi)$ enhancement is a coincidence of statistical fluctuations can be justifiably set aside. This is true also for the lobelike features; no experimental errors are known which could account for the observations. A model which simulates the structures in both the $M_{\mu\pi}$ and $M_{\mu\mu}$ distribution is based on the assumption that there is a cascade disintegration of $M^*_{\mu\pi}$ via a short-lived daughter particle:

$$M^*_{\mu\pi}\rightarrow\mu_1+M^*_{\mu\nu}\rightarrow\mu_1+\mu_2+\nu\ .$$

Alignment of $\mu_2$ with $\mu_1$ in the $M^*_{\mu\nu}$ c.m.s. causes lobes in the $M_{\mu\pi}$ distribution because of the experimental difficulty of separating $(\mu,\mu)$ from $(\mu,\pi)$. No alternative type of mechanism for lobe production has been found.

The method of analysis makes use of the two modes of decay of $M^*_{\mu\pi}$ and the fact that both products of the $(\mu,\pi)$ decay are measurable. If the only mode were via $M^*_{\mu\nu}$, there would be no reference enhancement in the mass distributions to enable the association of the lobes with $M^*_{\mu\pi}$ and, hence, their identification. This aspect is important for searches for other sources of production of $M^*_{\mu\pi}$ and other analogous daughter particles.

The scope of this paper has been restricted to the phenomenological evidence for the existence of a specific parent $M^*_{\mu\pi}$ and its daughter $M^*_{\mu\nu}$. No physical explanations of their existence are ventured. It may be useful, however, to recapitulate those observations which appear especially relevant to the development of such explanations and which might lead, also, to new experiments.

1. The masses of the $(\mu,\pi)$ and $(\mu,\nu)$ states are determined from enhancements in invariant-mass distributions with calibrated absolute mass scales:

$$M^*_{\mu\pi}=0.429\pm0.002\ \text{GeV}\ ,$$

$$M^*_{\mu\nu}=0.127\pm0.005\ \text{GeV}\ .$$

2. (a) The uncertainty in the lifetime $(\tau_{\mu\pi})$ of $M^*_{\mu\pi}$ is large. There is no observable flight path in bubble chambers; the assumption of a path $<1$ mm sets an upper limit of $10^{-12}$ sec. With an experimental mass resolution of $\sim0.002$ GeV, there is no detectable width. This sets the lower limit to the range: $10^{-21}<\tau_{\mu\pi}<10^{-12}$ sec.

(b) Neither is there evidence for a flight path of $M^*_{\mu\nu}$. However, the lower-mass lobe extends over a larger range in $M_{\mu\mu}$ than the higher-mass lobe, enabling a width of $0.005\pm0.003$ GeV to be assigned to $M^*_{\mu\nu}$. Thus, $\tau_{\mu\nu}\sim(3\pm2)\times10^{-21}$ sec from the lobes and $\tau_{\mu\nu}<10^{-12}$ sec because of the absence of a flight path.

3. The lobes would not have been noticed if their areas and amplitudes were not comparable with the $M^*_{\mu\pi}$ enhancement, i.e., if the rates of the $(\mu,\pi)$ decay and the $(\mu,\mu,\nu)$ cascade were not comparable. The branching ratio $(R)$ of the $(\mu,\mu,\nu)$ to $(\mu,\pi)$ mode is $2.5<R<5$.

4. Observations which indicate general features of angular distributions are the following.

(a) The $M^*_{\mu\pi}$ enhancement is more significant from $(\mu,\pi)$ selected so that $p_\mu>p_\pi$, rather than $p_\pi>p_\mu$. This means that in the c.m.s. of $M^*_{\mu\pi}\rightarrow(\mu,\pi)$, with respect to its LOF, the $\mu$ momentum is predominantly in the forward hemisphere.

(b) The $M^*_{\mu\pi}$ enhancement from $K^0_{\mu3}\rightarrow(\nu,M^*_{\mu\pi})$ is most significant in the $(\mu,\pi)$ with large transverse momentum. This means that in the c.m.s. of $K^0_{\mu3}$, $M^*_{\mu\pi}$ is produced

preferentially perpendicular to the LOF.

(c) The lobes are caused by the preferential alignment of $\mu_2$ with $\mu_1$ in the c.m.s. of $M^*_{\mu\nu}\to(\mu_2,\nu)$. That the lower-mass lobe is of greater area than the higher-mass lobe indicates that in this c.m.s. the major component of momentum of $\mu_2$ is parallel, rather than antiparallel to the LOF of $\mu_1$ from $M^*_{\mu\pi}\to(\mu_1,M^*_{\mu\nu})$. That the lower-mass lobe extends over a greater range in $M_{\mu\mu}$, compared with the upper-mass lobe, indicates that $M^*_{\mu\nu}$ has a width.

(d) The lobes from $K^0_{\mu3}$ experiments in the HLBC and HBC can be simulated when it is assumed that in the c.m.s. of $M^*_{\mu\pi}\to(\mu_1,M^*_{\mu\nu})$, with respect to its LOF, the direction of the normal to the decay plane of $M^*_{\mu\nu}$ is isotropic. Simulation of the type of lobes from the $\nu$ experiments requires the direction to the normal to the decay of $M^*_{\mu\nu}$ to be, preferentially, skew forward.

5. The study of the enhancement at 0.429 GeV arose from the correlations in the $M_{\mu\pi}$ distributions from different experiments. There is no evidence that the enhancement and the lobes are independent of a locally smooth background. There are also significant correlations in these distributions outside the region of the lobes indicated in this paper; there is no evidence that the phenomenology of $M^*_{\mu\nu}(0.127)$ is unique to $M^*_{\mu\pi}(0.429)$.

## ACKNOWLEDGMENTS

My warmest thanks are due to Mme. H. Cabel for the care she took to ensure that the data of early analyses are retrievable, and to Miss J. Semmens for her meticulous assistance with the data reduction and preparation for this paper. I remain deeply indebted to my colleagues and fellow members of the former NPA division of CERN and to the experimental groups who made available observations for these analyses. Without implication of their scientific opinions, I acknowledge particularly H. W. K. Hopkins, P. G. Innocenti, J. B. M. Pattison, K. J. Peach, and R. Stump; without their extensive help in the early data analysis these studies would not have been possible. I have valued also stimulating discussions with E. W. Vogt of possible physical indications from the model studies.

## APPENDIX

This appendix contains other details of $M_{\mu\pi}$ distributions which can be relevant for the design of new experiments.

### 1. Effects of some selections

Figures 15(a), 15(b), and 15(d) show difference histograms for selections of the HBC data, the captions are self-explanatory. The increase in statistical significance of the $M_{\mu\pi}$ enhancement for the selection $p_\mu=p_1$, compared with the distribution from both possible assignments of the $(\mu,\pi)$ is a property of all observations because of the preference for decay with $p_\mu>p_\pi$. For the indicated regions of (a), (b), and (d), respectively, $\chi^2_{17}=12.7$ (CLS=70%), $\chi^2_{14}=20.0$ (CLS=10%), and $\chi^2_{10}=27.0$ (CLS=$10^{-3}$). The increased $\chi^2$ in (d) is due, largely, to the reduction in $K^0_{e3}$ background. Histogram (c) is from preliminary data from a streamer chamber[20] and may be compared with (b). The $(\mu,\pi)$ are selected as those $V^0$ in which both tracks traverse Pb plates without interaction. This is an unfavorable selection for $\pi$ detection, but it reduces the $K^0_{e3}$ background. The indicated region is of low statistical significance: $\chi^2_{14}=17.6$ (CLS=17%). A correctly located $M^*_{\mu\pi}$ fluctuation can be assigned and there are some other indications of similarities with (b). In particular the appearance of relatively more amplitudes

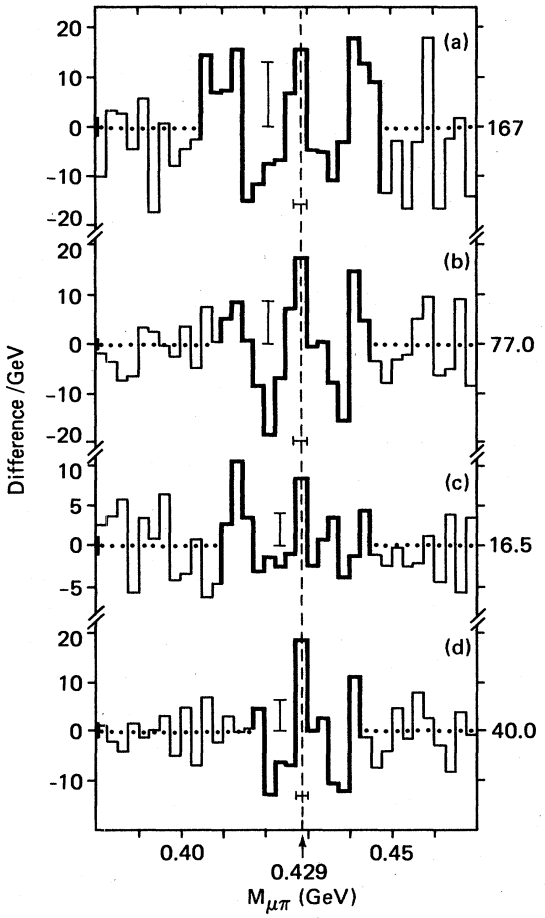


FIG. 15. Some effects of selection of $K^0_{\mu3}$ decays in the HBC and in a streamer chamber, in the vicinity of $M^*_{\mu\pi}$. (a) difference histogram from all $V^0$ from HBC, both $(\mu,\pi)$ assignments as in Fig. 6(a). For the indicated region, $\chi^2_{17}=12.7$ (CLS=70%). (b) removal of some $K^0_{e3}$ background with the selections $p_1/p_2<5$ and $p_\mu=p_1$. For the indicated region $\chi^2_{14}=20.0$ (CLS=10%). A sample of $M_{\mu\pi}$ from preliminary observations of some $10^4$ $K^0_L$ decays in a streamer chamber is shown in (c). These data are comparable to (b), also in mass scale calibration; they have been selected for $p_\mu=p_1$ from $V^0$ with tracks without interactions in Pb plates. For the indicated region, $\chi^2_{14}=17.6$ (CLS=17%); note the apparently greater number of events, relative to the $M^*_{\mu\pi}$ fluctuation, in the region corresponding to the lower-mass lobe in (b). This is compatible with a favorable selection for $(\mu,\mu)$ because of the noninteracting tracks. Further selection of (b) to $p_1/p_2<2$ in (d) is unfavorable for the extreme region of the lobes, but enhances the significance of the fluctuations in the region of $M^*_{\mu\pi}$: $\chi^2_{10}=27.0$ (CLS=$10^{-3}$).

in the lobes of (c) compared with the $M^*_{\mu\pi}$ fluctuation, referred to in Sec. VII, is compatible with the presence of some $(\mu,\mu)$ combinations.

### 2. Some detailed correlations

Despite the smoothness in terms of the usual $\chi^2$ of the observations for the difference histograms of Figs. 4(a) and 4(d), there are indications of correlations with other data, as can be seen also in the following tests. Suppose the direction of a bin edge is called "up" if the right bin is higher than the left, and conversely. It is evident that in a difference histogram, as distinct from a histogram, from a physically smooth distribution the directions of bin edges, and specifically, the directions of successive bin edges can be expected to be random.

Of the 35 pairs of corresponding bin edges across the difference histograms in Figs. 4(a) and 4(b), 26 pairs have the same direction. This results in $\chi^2=16.5$ (CL$=2\times10^{-3}$ for 1 degree of freedom) for the hypothesis that the directions of corresponding bin edges are random between the two diagrams. There is no immediately obvious similarity in the patterns of (a) and (b), the lack of randomness indicated in this $\chi^2$ test is compatible with the existence of narrow features which are smeared by shifts in calibration. If the 22 edges of the corresponding 21 indicated bins in Figs. 4(c) and 4(d) are compared, similarly, the directions are the same in 13 cases. The previous test would show that this is compatible with random directions in a corresponding pair of bin edges. However, 10 of the 11 pairs to the left of the $M^*_{\mu\pi}$ bin have the same directions and 7 of the 11 to the right have opposite directions. This situation might arise also if there were some small systematic shift in the location of patterns.

An illustration of effects of small displacements of patterns, which may be connected with such possibilities, is given in Fig. 16. Difference histogram (a), prepared as for Fig. 4, is from data I of Bisi *et al.* for $\cos\theta_{\mu\nu}<0$ in the original bins of 0.0025 GeV in $T_\nu$ shown against the $M_{\mu\pi}$ scale (Sec. II): $\chi^2_{18}=54.1$ (CLS$=10^{-5}$). Difference histogram (b) is from the same selection of data II, for which the experimental conditions were modified to accept a wider range of $p_T$. The accuracy of calibration of the mass scale for data I, which is within 0.003 GeV, and the resolution has been discussed in Sec. III. The calibration for data II is not stated, they are unlikely to have mass errors as small as data I because of the operation with a lower magnetic field. The invariance with respect to decay configuration may not be the same, either, because of the need for a different set of bending length corrections: no resolution function for data II is available. There is no $M^*_{\mu\pi}$ enhancement in (b), neither are the data smooth: $\chi^2_{18}=35.0$ (CLS$=6\times10^{-3}$), which may be compared with CLS$=56\%$ in Fig. 3(a) and 91% in Fig. 4(d). The remaining difference histograms in Fig. 16 are from combinations of the input data for (a) and (b) as described in the caption. For the combination which results in (e): $\chi^2_{18}=62.1$ (CLS$=5\times10^{-7}$) and the $M^*_{\mu\pi}$ fluctuation stands $\sim3$ SD above an estimate of the reference of the distribution. The sequential changes in the patterns in (d), (e), and (f) can lead to the question as to whether they

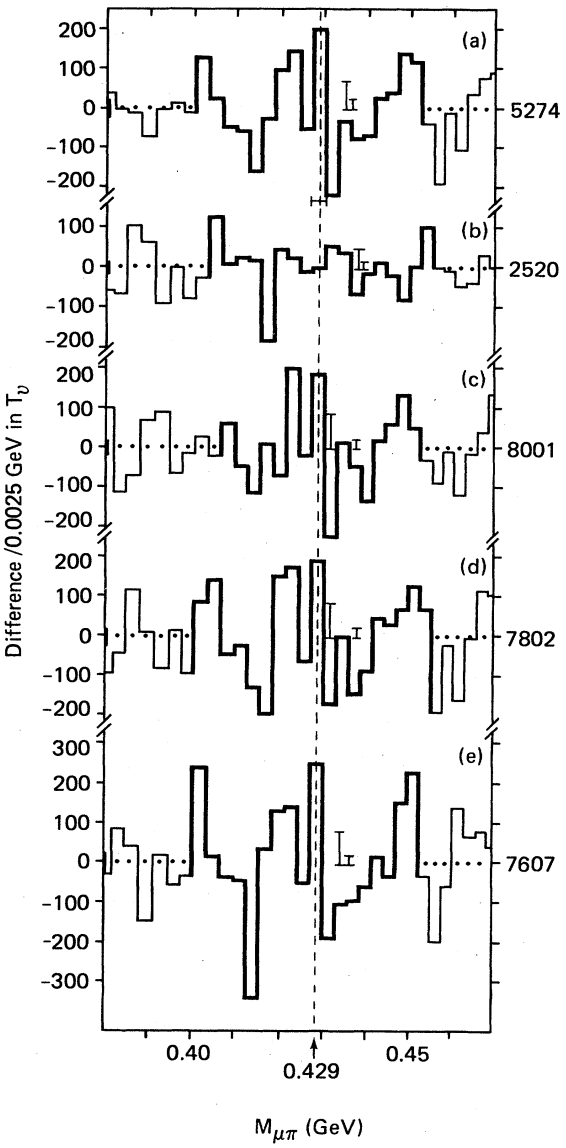


FIG. 16. Comparison and combination of data I and II of Bisi *et al.* for $\cos\theta_{\mu\nu}<0$, in the original bins of 0.0025 GeV in $T_\nu$. The difference histogram (a) may be compared with Fig. 4(c) which is in bins of 0.0025 GeV in $M_{\mu\pi}$. For the indicated region, $\chi^2_{18}=54.1$ (CLS$=10^{-5}$). Data II are presented in (b); for the indicated region, $\chi^2_{18}=35.0$ (CLS$=6\times10^{-3}$). The calibration is not stated, neither indicated region is smooth. Comparison of the fluctuations in (a) and (b) reveals some similarities, with effects which are evident in combinations of data I and II. Difference histogram (c) is from the combination of data II, displaced one bin to the right and added to data I, for the indicated region, $\chi^2_{16}=24.7$ (CLS$=5\%$). Similarly (d) is from data II added directly to data I, for the indicated region, $\chi^2_{19}=37.5$ (CLS$=5\times10^{-3}$); and (e) is from data II displaced one bin to the left and added to data I. For the indicated region, $\chi^2_{18}=62.1$ (CLS$=5\times10^{-7}$). The patterns in (e) and in Fig. 4(f) are similar; but (e) is of greater statistical significance. The sequence of $\chi^2_N$ in (c), (d), and (e), is compatible with a difference in mass scale calibrations between the two data sets.

could be due to differences in the mass scale calibration between data I and data II? Partly because of the greater average width of 0.0025-GeV bins in $T_\nu$, relative to those of 0.0025 GeV in $M_{\mu\pi}$, the pattern in Fig. 16(f) is more significant statistically, than any pattern in Fig. 4.

The addition of all data I and II gives a reference level, in values/GeV in the region of $M^*_{\mu\pi}$, greater than the level shown by Donaldson *et al.*, referred to in Sec. VII of (I). The statement of Donaldson *et al.* that there are no sharp departures from smoothness anywhere in their $M_{\mu\pi}$ spectrum, accords with the conclusion of Bisi *et al.*; but not with the analysis in Fig. 16. The report of the experiment of Donaldson *et al.* does not fulfill the criteria in Sec. V. It gives no demonstration of an observed line from a narrow decay, and the $M_{\mu\pi}$ distribution in their Fig. 24 is on a three-cycle-logarithmic ordinate which cannot be read back for an informative comparison with the experimental observations discussed here.

### 3. Questions concerning $p_T$

Almost all possible $K^0_{\mu 3}$ decay configurations are contained in the data from the HLBC and, specifically, the $(\mu,\pi)$ are from all possible values of $p_T$. For reference, the difference histogram from these data [Fig. 6(b)] is shown again in Fig. 17(b). In observations selected with $p_T \sim 0$ the $M_{\mu\pi}$ enhancement has not been seen, as in the case in the difference histogram from the observations of Clark *et al.* in Fig. 4(d). It was shown in that figure that the observations can be combined with those of Bisi *et al.* and the SC to yield a pattern of greater statistical significance around $M^*_{\mu\pi}$ than in any one of the individual observations. In the Appendix, section 2, other signs of correlations have been mentioned. Figure 17(a) shows again the difference histogram of Fig. 4(d), drawn so that enhancements are downward (N.B. the ordinate scale). The calibration errors in the observation of Clark *et al.* and also in the HLBC are $<0.002$ GeV and the $K^0_L$ momentum spectra are comparable. The three depletions indicated are of low statistical significance, from low to high mass: $\chi^2{}_2 = 3.4$, 0.9, and 1.4 (CLS = 10%, 40%, and 70%). However, if as for Fig. 6(d) these features are considered as the most significant three of the fluctuations in their direction, and if they are expected to be randomly distributed across the diagram, the probability is $<1\%$ for their simultaneous occurrence within, say, $\pm 2$ bins of their actual locations above the enhancements and lobes in (b). If this situation is not fortuitous, it might be asked in further experiments to what extent there may be some conservation of the $M_{\mu\pi}$ distribution from $K^0_{\mu 3}$: are some selections for, e.g., $p_T > 0$ related to depletions for $p_T \sim 0$?

Difference histograms (c), (d), and (e) are also concerned with transverse momentum: they show the differences between the observed and calculated frequencies of the distribution of transverse momentum of the $\nu$ in tests[26] of consistency of observations in an experiment[27] to measure charge asymmetry from some $0.96\times 10^8$ $K^0_{e3} \rightarrow (e,\pi,\nu)$ decays. For convenience of comparison the original scale in $p_T$ of the $\nu$ has been converted to a scale of $M_{\mu\pi}$, the reading error bar is shown. The samples of $p_T$ values for (c) and (d) are equal and nonoverlapping, from Figs. 9(a) and 9(b), respectively, in the thesis of R.

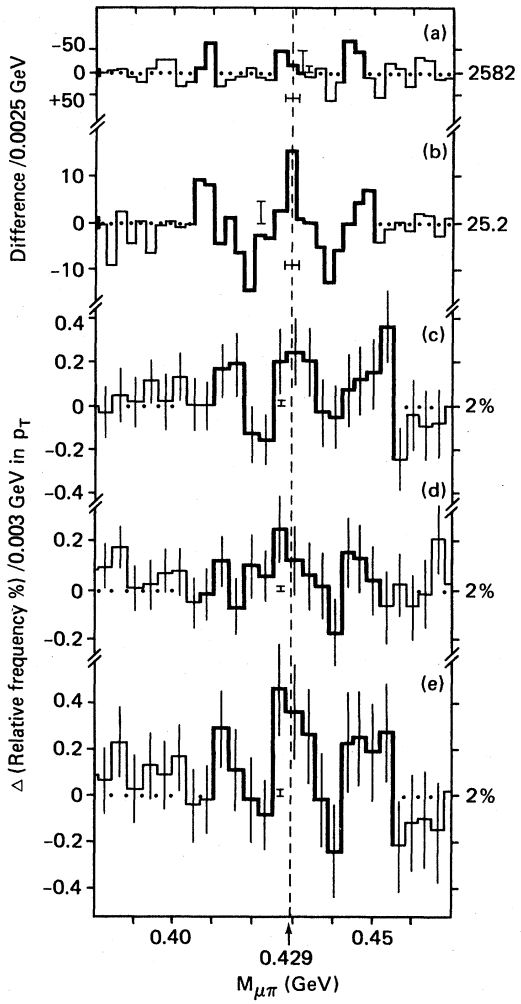


FIG. 17. $M_{\mu\pi}$ distributions with different selections in $p_T$: the difference histogram from the data of Clark *et al.* ($p_T \sim 0$), shown already in Figs. 4(d) and 6(f), is redrawn in (a), with depletions upward (note the ordinate). Difference histogram (b) is from the HLBC [Fig. 6(b)] where all possible $K^0_{\mu 3}$ configurations are detected, the $K^0_L$ momentum spectrum is similar to that for Clark *et al.* Using the test for Fig. 6(d), the probability is $<1\%$ that the "most conspicuous 3" depletions in (a) should resemble the pattern of the upward fluctuations in (b). Future experimental studies of the angular distribution of the $K^0_{\mu 3}$ decays might investigate whether, as a consequence of the preferred production of $M^*_{\mu\pi}$ with $p_T \sim p_T\text{max}$, there are actual depletions in $M_{\mu\pi}$ distributions with $p_T \sim 0$? Histograms (c) and (d) are differences from a Monte Carlo calculation for nonoverlapping, equal samples of the observed frequency distribution of $p_T$ of the $V^0$ from an experiment to study $K^0_{e3} \rightarrow (e,\pi,\nu)$. Difference histogram (e) is from the combination of these data; the ordinates in each diagram are in percentages/sample. For the indicated region, $\chi^2{}_{13} = 20.7$ (CLS = 6%). However, the probability is $<10^{-4}$ that the largest fluctuations throughout the entire range ($0 < p_T < 0.15$ GeV/$c$) of these two samples of the $p_T$ distribution should be statistical fluctuations so located as to resemble the pattern of an enhancement of $M^*_{\mu\pi}$ and two lobes. If this pattern is not due to statistical fluctuations, to what extent could it be due to the preferred production orientation of $M^*_{\mu\pi}$ of $p_T \sim p_{T\max}$ in either the decays of $K^0_{e3}$, which the experiment was designed to study, or in a $K^0_{\mu 3}$ background?

C. Webb; (e) represents their combination. The departures from the smooth Monte Carlo calculations in Fig. 17 are the largest over the range $0<p_T<0.150$ GeV/$c$ of the original distributions which, although not stated, appear to have $\sim 500$ values in the $M^*_{\mu\pi}$ bin in (e). For the indicated region in (c), $\chi^2_{13}=20.7$ (CLS=10%); in (d), $\chi^2_{14}=11.6$ (CLS=50%); and in (e), $\chi^2_{13}=20.7$ (CLS=6%). The fluctuations are not mentioned by the author; for the aims of the experiment the observed overall distributions may be considered in general accord with the calculations.

However, the probability is $<10^{-4}$ that the largest fluctuations in the independent samples in the diagrams should be located as they are with respect to $M^*_{\mu\pi}$, be mutually compatible, and combine to give the pattern in (c). Furthermore, this pattern can be compatibly placed in the series of patterns in Fig. 6. Only the momenta of the components of the $V^0$ pair, without identification of masses, are needed to determine $p_T$. If these patterns are not a statistical effect, or do not have some other known explanation it may be asked (i) whether the preferred $M^*_{\mu\pi}$ orientation of $p_T\sim p_T\max$ is the cause of these patterns? and (ii) if they are due to such a cause, are the $M^*_{\mu\pi}$ produced from $K^0_{\mu 3}$ contamination in the experiment, or might they originate from the $K^0_{e3}$ which the experiment is designed to study?

---


[1]C. A. Ramm, Phys. Rev. D **26**, 27 (1982).

[2]C. A. Ramm, Nature **227**, 1323 (1970).

[3]K. J. Peach made available $M_{\mu\pi}$ distributions from the experiment described in G. R. Evans, M. Golden, J. Muir, K. J. Peach, L. A. Budagov, H. Hopkins, W. Krenz, F. Nezrick, and R. G. Worthington, Phys. Rev. Lett. **23**, 427 (1969).

[4]For the needs of this paper the fitting parameters of the polynomials are not critical. The minimum useful degree is visually obvious from a plot with respect to the data, and numerically obvious as the degree for which the ratio of the residual sum of the squares to the variance ($F$ value) ceases to fall sharply. There is no increase in statistical significance of the overall fit beyond this degree, but the choice of a higher value may change the accommodation of the polynomial to some given range of the data. This aspect is considered for the difference histograms in, e.g., Fig. 4 and for the levels of references calculated with gaps in the data, such as for the crosses in Fig. 5. Over the range in abscissas of all diagrams in this paper the polynomial references are, of course, visually smooth and, except for the special purpose of Fig. 13, without a point of inflexion.

[5]H. W. K. Hopkins made available $M_{\mu\pi}$ distributions from the experiment described in H. W. K. Hopkins, T. C. Bacon, and F. R. Eisler, Phys. Rev. Lett. **28B**, 215 (1968).

[6]A. R. Clark, T. Elioff, H. J. Frisch, R. P. Johnson, L. T. Kerth, G. Shen, and W. A. Wenzel, Phys. Rev. D **9**, 533 (1974).

[7]P. G. Innocenti made available data tapes and C. D. Buchanan a preliminary $M_{\mu\pi}$ distribution from the experiment described in C. Y. Chien, B. Cox, L. Ettlinger, L. Resvanis, R. A. Zdanis, E. Dally, P. Innocenti, E. Seppi, C. D. Buchanan, D. J. Drickey, F. D. Rudnick, P. F. Shephard, D. H. Stork, and H. K. Ticho, Phys. Lett. **33B**, 627 (1970).

[8]C. A. Ramm, Nuovo Cimento **16A**, 47 (1973).

[9]V. Bisi, M. Cullen, P. Darriulat, C. Grosso, M. I. Ferrero, E. Radermacher, C. Rubbia, D. Shambroom, A. Staude, and K. Tittel, CERN Report No. D.Ph 1, 1970 (unpublished).

[10]H. Foeth, M. Holder, E. Radermacher, A. Staude, P. Darriulat, J. Deutsch, K. Kleinknecht, C. Rubbia, K. Tittel, M. I. Ferrero, and C. Grosso, Phys. Lett. **30B**, 282 (1969).

[11]A. R. Clark, T. Elioff, R. C. Field, H. J. Frisch, R. P. Johnson, L. T. Kerth, G. Shen, and W. A. Wenzel, Nature **237**, 388 (1972).

[12]C. A. Ramm, CERN Report No. Addendum 6-NPA 69-6, 1971 (unpublished).

[13]The definition of $p_1>p_2$ refers only to the laboratory momenta. If the particles of the combination are $A$ and $B$, of similar mass and their c.m.s. has $\beta\sim 1$, the angle $\theta^*$ between the momentum $\mathbf{p}^*$ of $A$ in the c.m.s. and its line of flight is such that

$$\cos\theta^*\sim\frac{E^*}{p^*}[(p_A/p_B)-1]/[(p_A/p_B)+1]\,,$$

where $p_A$ and $p_B$ are the respective laboratory momenta. Thus the restriction $p_1/p_2<2$ selects the range $-0.3\le\cos\theta^*\le 0.3$.

[14]K. J. Peach made available $M_{\mu\pi}$ distributions from the experiment described in L. Bertanza, W. Cameron, P. Capiluppi, P. Croft, E. Flaminio, R. Jennings, G. Kalmus, P. Lugaresi-Serra, G. Mandrioli, A. Minguzzi-Ranzi, W. Morton, A. Nappi, R. Pazzi, K. J. Peach, A. M. Rossi, B. Saitta, and W. Venus, Nucl. Phys. **B110**, 1 (1976).

[15]Y. Cho, M. Derrick, R. J. Miller, J. Schlereth, A. Engler, G. S. Keyes, R. W. Kraemer, and M. Tanaka, Phys. Rev. D **22**, 2688 (1980).

[16]A. Engler, G. Keyes, R. W. Kraemer, M. Tanaka, Y. Cho, M. Derrick, D. Lissauer, R. J. Miller, J. Schlereth, and R. P. Smith, Phys. Rev. D **18**, 3061 (1978).

[17]H. C. Ballagh, H. H. Bingham, T. J. Lawry, G. R. Lynch, J. Lys, M. L. Stevenson, F. R. Huson, E. Schmidt, W. Smart, M. D. Sokoloff, E. Treadwell, R. J. Cense, F. A. Harris, M. D. Jones, A. Koide, S. I. Parker, M. W. Peters, V. Z. Peterson, H. J. Lubatti, K. Moriyasu, E. Wolin, U. Camerini, W. Fry, D. Gee, M. Gee, R. J. Loveless, and D. D. Reeder, Phys. Rev. D **29**, 1300 (1984).

[18]C. A. Ramm, University of Melbourne report, 1983 (unpublished).

[19]G. Bernadini, H. Bienlein, A. Bohm, G. von Dardel, H. Faissner, F. Ferrero, J.-M. Gaillard, H. J. Gerber, B. Hahn, M. Holder, V. Kaftanov, F. Krienen, C. Manfredotti, M. Reinharz, R. A. Salmeron, A. Staude, H. J. Steiner, J. Bartley, M. M. Block, H. Burmiester, D. C. Cundy, B. Eiben, C. Franzinetti, J. Keren, R. Møllerud, G. Myatt, M. Nickolič, A. Orkin-Lecourtois, M. Paty, D. H. Perkins, C. A. Ramm, K. Schultze, H. Sletten, K. Soop, R. Stump, W. Venus, and H. Yoshiki, Nuovo Cimento **38**, 608 (1965).

[20]R. Mozley and his group made available the $M_{\mu\pi}$ distribution from preliminary experiments with $K^0_L$ decays in their

streamer chamber.
[21]J. LeBritton, D. McCal, A. Melissinos, W. Metcalf, M. Miller, J. Alspector, S. Borenstein, G. Kalbfleisch, J. Scharenguivel, R. Strand, and A. Abashian, Phys. Rev. D **23**, 1 (1981).
[22]J. Badier, J. Boucrot, J. Bourotte, G. Burgun, O. Callot, Ph. Charpentier, M. Crozon, D. Decamp, P. Delpierre, B. Gandois, R. Hagelberg, M. Hansroul, Y. Karyotakis, W. Kienzle, P. Le Dû, J. Lefrançois, Th. Leray, J. Maillard, A. Michelini, Ph. Miné, G. Rahal, O. Runolfsson, P. Siegrist, A. Tilquin, J. Valentin, R. Vanderhaghen, and S. Weisz, Phys. Lett. **122B**, 441 (1983).
[23]T. D. Lee and C. N. Yang, Phys. Rev. Lett. **4**, 307 (1960).
[24]T. D. Lee and C. N. Yang, Phys. Rev. **119**, 1410 (1960).
[25]C. A. Ramm, Nature **230**, 145 (1971).
[26]R. C. Webb, Ph.D. thesis, Princeton University, 1972.
[27]V. L. Fitch, V. Hepp, D. Jensen, M. Strovink, and R. C. Webb, Phys. Rev. Lett. **31**, 524 (1973).